MICROFLUIDIC DETECTION OF WATERBORNE PATHOGEN THROUGH LIGHT SCATTERING OF PARTICLE IMMUNOASSAYS

by

Jin-Hee Han

A Dissertation Submitted to the Faculty of the

DEPARTMENT OF AGRICULTURAL & BIOSYSTEMS ENGINEERING

In Partial Fulfillment of the Requirements

for the Degree of

DOCTOR OF PHILOSOPHY

In the Graduate College

THE UNIVERSITY OF ARIZONA

2008

THE UNIVERSITY OF ARIZONA
GRADUATE COLLEGE

As members of the Dissertation Committee, we certify that we have read the dissertation

prepared by Jin-Hee Han

entitled MICROFLUIDIC DETECTION OF WATERBORNE PATHOGEN THROUGH LIGHT SCATTERING OF PARTICLE IMMUNOASSAYS

and recommend that it be accepted as fulfilling the dissertation requirement for the

Degree of Doctor of Philosophy.

_____ Date: 07/07/08
Dr. Jeong-Yeol Yoon

_____ Date: 07/07/08
Dr. Donald C. Slack

_____ Date: 07/07/08
Dr. Christopher Y. Choi

_____ Date: 07/07/08
Dr. Joel L. Cuello

Final approval and acceptance of this dissertation is contingent upon the candidate's submission of the final copies of the dissertation to the Graduate College.

I hereby certify that I have read this dissertation prepared under my direction and recommend that it be accepted as fulfilling the dissertation requirement.

_____ Date: 07/07/08
Dissertation Director: Dr. Jeong-Yeol Yoon

STATEMENT BY AUTHOR

This dissertation has been submitted in partial fulfillment of requirements for an advanced degree at the University of Arizona and is deposited in the University Library to be made available to borrowers under rules of the Library.

Brief quotations from this dissertation are allowable without special permission, provided that accurate acknowledgment of source is made. Requests for permission for extended quotation from or reproduction of this manuscript in whole or in part may be granted by the head of the major department or the Dean of the Graduate College when in his or her judgment the proposed use of the material is in the interests of scholarship. In all other instances, however, permission must be obtained from the author.

SIGNED: Jin-Hee Han

ACKNOWLEDGEMENTS

I would like to express appreciation and gratitude to my advisor, Dr. Jeong-Yeol Yoon, for sharing his knowledge and inspiring me to do this research. Dr. Yoon always gave me the right direction to complete each projects and share his precious time to have in-depth conversation with me about research as well as life in general.

I want to thank to my committee members Dr. Donald Slack, Dr. Christopher Choi, and Dr. Joel Cuello for their support, feedback, and guidance during my time at the university.

I also wish to thank the members of the Biosensors Lab (BSL) for all their help and moral support including Tremaine Powell, Brian Heinze, Jennine Chesler, and Dr. Keesung Kim. I could have excellent collaboration ship and private relationship with the members in the BSL. It was one of the most precious time in my life

Most of all, I deeply appreciate supports and love from my wife Eun, and my parents Sung-Bong and Jung-Ja. In addition, I want to share this moment with my newborn baby, Celline.

DEDICATION

I dedicate this work to the grace of my God.

TABLE OF CONTENTS

TABLE OF CONTENTS- *Continued*

LIST OF FIGURES

ABSTRACT

This dissertation focused on detecting waterborne pathogens in a microfluidic biosensing system which enables point-of-care, real-time monitoring. Within this framework, I have been addressing three objectives.

The first objective was to enhance mixing of particles in a microfluidic device. To this end, SDS (sodium dodecyl sulfate) or Tween 80 (polyethylene sorbitol ester) was added to the antibody-conjugated polystyrene microparticle suspension. Both surfactants showed non-specific binding (with SDS) or very poor diffusion (with Tween 80). As an alternative approach, highly carboxylated polystyrene microparticles showed very low non-specific binding comparable to that with Tween 80 and good diffusional mixing equivalent to that with SDS. This work was published in Appendix A (© 2008 Elsevier).

The second objective was to detect *E. coli* K-12 using the microfluidic-based system with low detection limit in Appendix B (© 2008 Elsevier). This method was essentially one-step and requires no sample pre-treatment or cell culturing. Conventional immunoassay using polyclonal antibody detects not only viable cells, but also dead cell and free antigens. In order to reduce false positive signal originated from dead cells and free antigens, target solution was washed three times. The detection limit was as low as 40 cfu ml^{-1} or 4 cfu per device (viable cells only), or <10 cfu ml^{-1} or <1 cfu per device (including dead cells and free antigens).

Our final objective was to develop real-time, high sensitive method for detecting waterborne pathogens in a water distribution system in Appendix C. Detection of *Escherichia coli* (*E. coli*) in a single straight pipe was demonstrated using a microfluidic

system utilizing light scattering detection of latex immunoagglutination assay. Assay time is <5 min per assay and detection limit is 10 cfu ml^{-1}. Optical signals are compared with viable *E. coli* counts (not real time) and salt tracer experiments. Laminar (Re = 1,102) and turbulent (Re = 6,144) flows are used to simulate the flow regimes in a real water distribution system.

INTRODUCTION

1. Overview of dissertation

This dissertation is a compilation of four studies which have been conducted between 2006 and 2008. The first published paper of this study (Appendix A) describes the method to enhance diffusional mixing toward a successful particle-based immunoagglutination assay in a microfluidic device. Latex immunoagglutination assay has been popular in medical diagnostics due to its simplicity. There is also growing interest in conducting multiple immunoassays in a microfluidic device for real-time, high-throughput assay. It is therefore logical to pursue latex immunoagglutination assay in a microfluidic device, but such a demonstration has had a limited success due to the mixing problem within microchannels. The mixing problem originates from; (1) strict laminar flow condition due to low Reynolds number in a microchannel, (2) the large size of the particles (1–10 μm) and particularly their agglutinates used in latex immunoagglutination assays

The primary goal of this study is to improve diffusional mixing towards the successful latex immunoagglutination, without any non-specific binding, under the laminar flow conditions. The other objective is to develop an immunosensing microfluidic device potentially useful for environmental pathogen monitoring.

To improve the latex immunoagglutination assay in a microfluidic device, we first use SDS (sodium dodecyl sulfate) and Tween 80 (polyethylene sorbitol ester). SDS or Tween 80 was added to the antibody-conjugated PS particles, which were mixed with the

target antigen solutions in a Y-junction microfluidic device. Alternatively, highly carboxylated PS particles without surfactant were also evaluated for the same type of experiments.

SDS shows non-specific binding (with SDS) and Tween 80 shows mixing difficulty. But, highly carboxylated particle without surfactant provides efficient mixing of solution and reagent solution and prevents non-specific binding.

The second published paper (Appendix B) describes detection of ***Escherichia coli*** (***E. coli***) using light scattering of latex immunoagglutination in a polydimethylsiloxane (PDMS) microfluidic device. Accidental outbreaks of waterborne pathogens have recently increased in drinking and irrigation water; consequently, a growing interest in developing more effective methods for detecting waterborne pathogens has arisen. Conventional detection methods prove to be time-consuming due to sample preparation and the need for pre-culturing samples. Although there have been several microfluidic-based methods to detect waterborne pathogens, their detection limit was over than 100 cfu ml^{-1}. Therefore, a better method is needed to detect solely viable target bacteria or viruses, with greater sensitivity, and in a simpler way.

In this study, we are using "proximity" optical fibers (i.e. the fibers are in close contact but not touching the microfluidic device) to quantify increased light scattering due to latex immunoagglutination in a microfluidic device. In order to reduce false positive signals caused by antibodies binding to non-viable *E. coli* cells or free antigens in solution, target solutions were washed three times, and then the results were compared to non-washing treatments.

Our microfluidic detection system shows real-time monitoring of *E. coli* with extremely high sensitivity (40 cfu ml^{-1} or 4 cfu per device of only viable cells), which are superior to the other results of the *E. coli* detection performed in microfluidic device.

The third paper (Appendix C) describes light scattering detection of latex immunoagglutination assay to monitor *E. coli* in a pipe flow.

The first goal of our study is to develop a real-time microfluidic system for detecting *E. coli* in pipe flows. Our central hypothesis is that light scattering detection of latex immunoagglutination assay can detect *E. coli* at very low detection limit using a single pipe microfluidic system. we monitor *E. coli* concentrations against time; along with both laminar and turbulent flows. The final objective is to compare the flow characteristics of *E. coli* obtained by this light scattering with those of salt tracer and the results of conventional *E. coli* cell counting (not real-time) to indentify differences between biological and non-biological agent in a pipe flow.

Laminar and turbulent flows are used to simulate the flow regimes in a real water distribution system. Water samples are collected from downstream end of pipe in sequence by automatic sampler and analyzed with the microfluidic system. Our microfluidic system consists of a microfluidic device and a miniature spectrometer utilizing light scattering detection of immunoagglutination assay.

Detection can be made in real time (<5 min per each assay), and at extremely low detection limit (10 cfu ml^{-1}), suggesting that the system is appropriate for monitoring waterborne pathogens in a water distribution system. Cell fragments and free antigens of *E. coli* behave similar to salt tracer (axial dispersion), while viable *E. coli* cells behave

very difficulty (with no axial dispersion). Self motility and pipe-wall-fouling of *E. coli* cannot create axial dispersion phenomena for Re = 1,102 and Re = 6,144.

2. Introduction to microfluidics

2.1 What is microfluidics?

There are several advantages of scaling down standard laboratory by a factor of 1000 or more from the decimeter scale to the few micrometer scale. One primary advantage is the dramatic reduction in the amount of required sample. Small volumes allow for very fast analysis, efficient detection schemes, and analysis. Moreover, the small volume makes it possible to develop compact and portable systems that might ease the use of bio/chemical handling and analysis systems tremendously [1]. In 1980s, microelectromechanical systems (MEMS) were developed integrating mechanical, fluidic, electromechanical, or thermal functions. In 1990s, the uses of MEMS devices were diversified to chemical, biological, and biomedical applications. These MEMS devices may use fluid flowing which is operating under different hydraulic conditions from that of macroscale fluid, leading to the need for the new research area, i.e. microfluidics.

Microfluidics can be defined as the study of flows that are simple or complex, mono- or multiphasic, which are circulating in artificial microsystems, i.e. systems that are fabricated using new technology [2].

2.2 Fabrication technique for microfluidics – Soft lithography

Soft lithography is the collective name for a set of new techniques: replica molding (REM), micro-transfer molding (μTM), micromolding in capillaries (MIMIC), solvent-assisted micromolding (SAMIM), and near field conformal photolithography using an eleastomeric phase shifting mask. All these methods use a patterned elastomer as a stamp, mold, or mask to generate micropatterns and microstructures instead of a rigid photomask. Soft lithography can generate structures as small as 30 nm. The major advantage of soft lithography is very fast procedure of fabrication. Fabrication takes less than 24 hours from design to production. Another advantage is low in cost and soft lithography is applicable to almost all polymers and thus to many materials (e.g. carbon, glasses) [3].

Replica molding (REM)

Replica molding is an efficient method for the duplication of the information (i.e. shape, morphology, and structure) present in the surface of a mold [4]. The value of replica molding is as a replication method: it allows duplication of three-dimensional topologies in a single step; it also enables duplication of complex structures in the manner in multiple copies with nanometer resolution in a simple, reliable, and inexpensive way [5].

Figure 1 shows the schematic of REM. The master mold is replicated in PDMS by casting and curing the PDMS pre-polymer. This negative replica is then oxidized using an oxygen plasma for 1 min and exposed to fluorinated silane for 2 hr to provide a

surface with low adhesion to PDMS. PDMS is then case against this negative replica, cured, and peeled away to reveal a positive replica of the original master [3].

Micro-transfer molding (μTM)

In figure 2, a thin layer of liquid prepolymer is applied to the patterned surface of a PDMS mold and the excess liquid is removed by scraping with a flat PDMS block or by following off with a stream of nitrogen [6]. This mold filled with prepolymer is then contacted to the substrate and the prepolymer is cured by exposing UV light. After the mold is peeled off, a patterned structure is created on the substrate. The thickness of a patterned structure is less than 100 nm. This thin film can be removed by using O_2 RIF.

Micromolding in capillaries (MIMIC)

In micromolding in capillaries (MIMIC), as shown in figure 3, the rubber stamp is pushed up against a substrate, and liquid is dropped to the end of the channels. After eliminating excess polymer, the polymer is cured, and stamp is removed. MIMIC has been used to fabricate all plastic field effect transistors [7] and in the fabrication of Pt-Si Schottky diodes [8].

Solvent-assisted micromolding (SAMIM)

A PDMS mold is wetted with the solvent and then contacted with the surface of the supporting substrate as shown in figure 4. The solvent dissolves a thin layer of the substrate, and the resulting fluid or gel is molded against the relief structure in the mold.

When the solvent is evaporated, the fluid creates a patterned structure complementary to that in the surface of the mold [5]. The solvent should have a relatively high vapor pressure and a moderately high surface tension to ensure rapid evaporation of the excess solvent and minimal selling of the PDMS mold [5].

2.3 Biological application of microfluidics

Single-Cell analysis on microfluidic device

Analysis of single cell enables greater discrimination of different types of cells and components housed within them. However traditional macroscopic techniques (e.g. flow and laser scanning cytometry, automated microscope etc.) have a very limited success to analyze a single cell [9].

Small size of microchannel (1-100 μm) is compatible with the sizes of biological cell, providing many advantages in the analysis of a single cell: (1) Laminar flow in microchannel enables reproducible, diffusion-limited mixing, which can be used to tailor the fluid exposure over the surface of a single cell [10], (2) The ability to manipulate very small, encapsulated volumes with pumps and valves increases the efficiency for reagent usage while minimizing the opportunity for contamination [11], and (3) The small volume allows for high sensitive detection with single cell level [12].

Microreactor

Microfluidic microreactor offer new opportunity due to inherent parallel processing, integrated sensing, and automation afforded lab-on-a chip formats [9].

Microreaction technology has great ability to product chemical. The high heat and mass transfer rates possible in microfuidic systems provide higher yields than those with conventional reactors [13]. The ability of incorporating sensitive and fast temperature measurements on a single chip lead to better separation and reaction control [9]. For these reasons, microreactor using microfluidic device has been widely employed in nucleic acid analysis, mapping of protein, enzyme catalysis

Cell sorting

Cell sorting is always hot issue for the scientists who are working on biochemical, pharmaceutical, and clinical studies. Cell sorting can be used to analyze the effects of drugs, research chemotherapy. Monitoring viral antigen is also possible using cell sorting. However, cell sorting has a hard issue that cells, especially mammalian cell has known to be highly heterogeneous in their genetic, proteomic, and behavioral characteristics [14]. To secure the accurate result in handling cells, highly enriched or clonal populations are needed to reduce cellular heterogenesity [15]. Although microscopy, polymerase chain reaction (PCR), patch clamp, and microanalytical chemical separation have been used, these methods have a limited success considering complex, labor- and time-consuming procedure in cell sorting. Alternatively, microfluidic based-lab-on-a chip can be used to integrate entire procedure of cell sorting which is automatically performed on a single chip. Recently, two methods of fluorescence activated cell sorter and magnetic filtration have been commonly used with lab-on-a chip [16].

Real-time, point-of-care detection using microfluidic device

Conventional laboratory-based methods (e.g. PCR, ELISA) has required lots of time for preparing sample prior to detect target pathogens. For this reason, diagnosis has been impossible in real fields. But, now microfluidic device is making successful story in clinical diagnosis with real-time detection and high sensitivity. This miniaturized device is integrating multiple biochemical analysis (e.g. PCR, cell lysis, cell separation) on a single platform. Automatic, point-of-care detection using microfluidic device is leading to revolution in human/animal clinics, food and water safety.

3. Immunoassay

An immunoassay is a biochemical test that measures the concentration of a substance in a biological liquid, typically serum or urine, using the reaction of an antibody or antibodies to its antigen [17]. Most of assay use the specificity of antigen/antibody biding to detect target pathogens. Recently, this immunoassay has been popularly employed in the fields of clinical practice, veterinary medicine, horticulture and agriculture, food industry, and environment health. Therefore, understanding immune response is prerequisite to develop detection methods for various pathogens.

3.1 The antigen-antibody reaction

Antigen recognition

The N-terminal 110 amino acid residues of both the light and heavy chain of immunoglobulin molecules are variable in sequence and interact with each other through multiple non-covalent interactions to generate the antigen binding site as shown in figure 5. While some thirty amino acids are potentially available as contact residues, for antigen, x-ray crystallographic studies of antibody/protein antigen complexes have shown a maximum of seventeen residues to be directly involved in binding contact. The number of amino acid residues of a protein antigen that are bound by antibody is similary restricted so that the average protein molecules will have on its surface many structurally dissimilar antigenic determinants or epitopes. It has been shown that 5-10 amino acid peptides representing a sequence within an intact protein can constitute an epitope. Such an eiptope is referred to as continuous because the residues are in continuous peptide

linkage in the protein. Other epitopes are termed discontinuous because the residues recognized by the antibody are in spatial proximity to each other within the three dimensional structure of the native protein, but are not in continuous peptide linkage within its primary structure. [18]

Properties of antibody

Antibody affinity is the strength of reaction between an single antigenic determinant and a individual binding site on the antibody. Avidity is a measure of the overall strength of binding of an antigen with many antigenic determinants and multivalent antibodies [19]. The practical manifestation of the ability of an antibody or antiserum to bind its antigen is evaluated in terms of its avidity [18].

Specificity is the ability of an individual antibody combining to a single antigen determinant or the ability of a population of antibody molecules to react with only one antigen. The specificity is the hallmark of an antibody. On the other hand, cross reactivity refers to the ability of an individual antibody combining site to react with more than one antigenic determinant or the ability of a population of antibody molecules to react with more than one antigen [19]. The cross reactivity is relevant to the use of anti-immunoglobulins as secondary reagents in certain types of immunoassay.

3.2 Immunoassay using latex particles

The most important issue is the high interaction between an antibody and corresponding target antigen. Appropriate concentration of antibodies and antigens leads

to a visible precipitate with human eyes or microscope. But the concentration of reagents is usually too low to monitor antibody/antigen reaction in assay. Alternatively, this issue can be resolved by labeling the antigen or antibody with particles or compounds.

Immunoassay using latex particles uses the agglutination of antibody- or antigen conjugated polystyrene spheres. Existence of complimentary antigens in the specimen results in connecting two or more particles (i.e. agglutination) as shown in figure 6. These agglutinates can be identified with naked eye.

To successfully accomplish latex agglutination test, some parameters should be considered: The characteristics of the polymer colloids in terms of size, surface charge, hydrophilic/ hydrophobic nature, or functional groups that may react with proteins; pH, ionic strength, nature of solved ions, temperature, presence of dehydrating agents for agglutination assay; the optical techniques used for the assay [20]. Further, false positive binding of particles due to destabilization of antibody-conjugated particles in aqueous solutions or response of dead cell and free antigens from target sample to polyclonal antibodies must be taken into account [12]. Otherwise, false positive binding leads to considerable erroneous diagnosis.

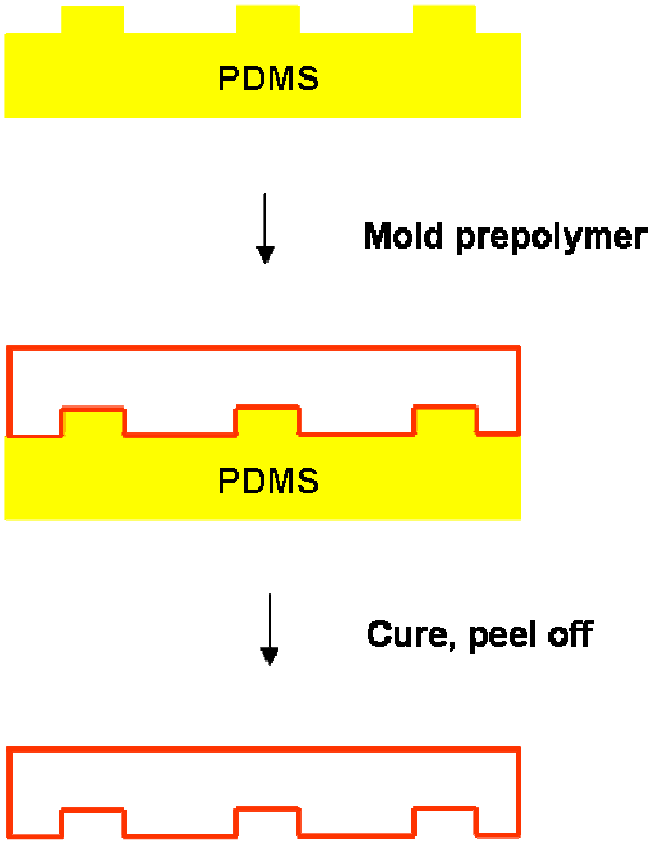

Figure 1. Schematic description of replica molding (REM)

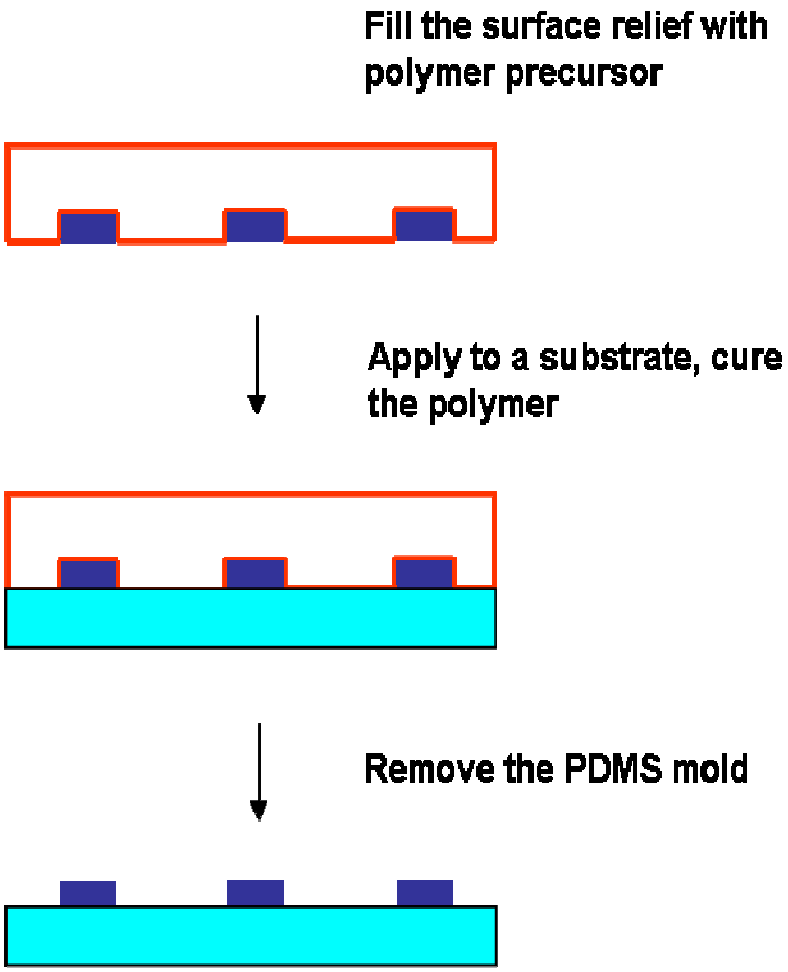

Figure 2. Schematic description of micro-transfer molding (μTM)

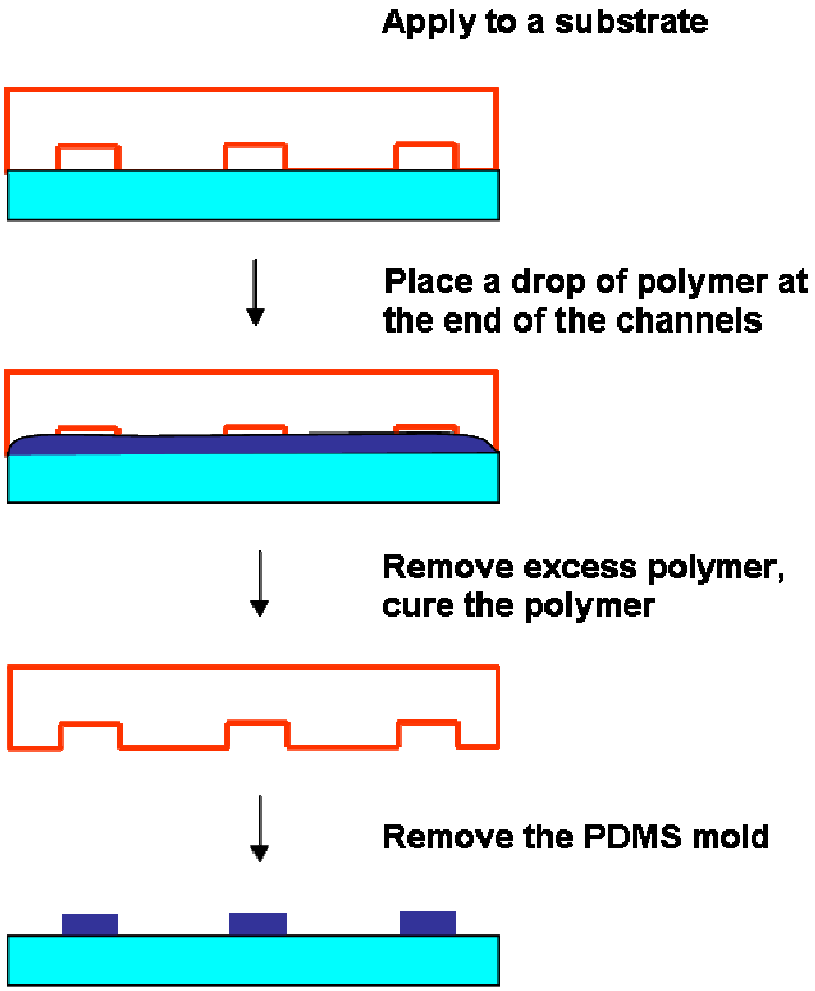

Figure 3. Schematic description of micromolding in capillaries (MIMIC)

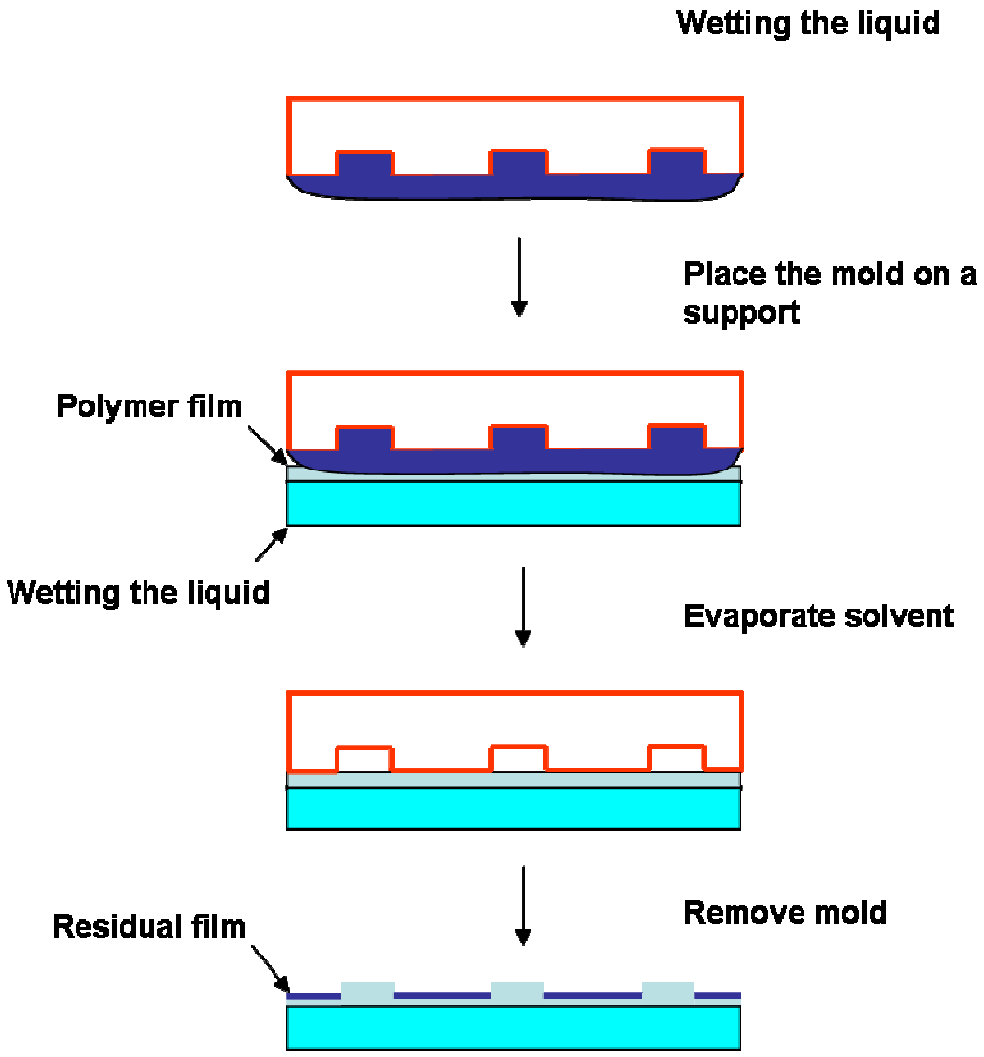

Figure 4. Schematic description of solvent-assisted micromolding

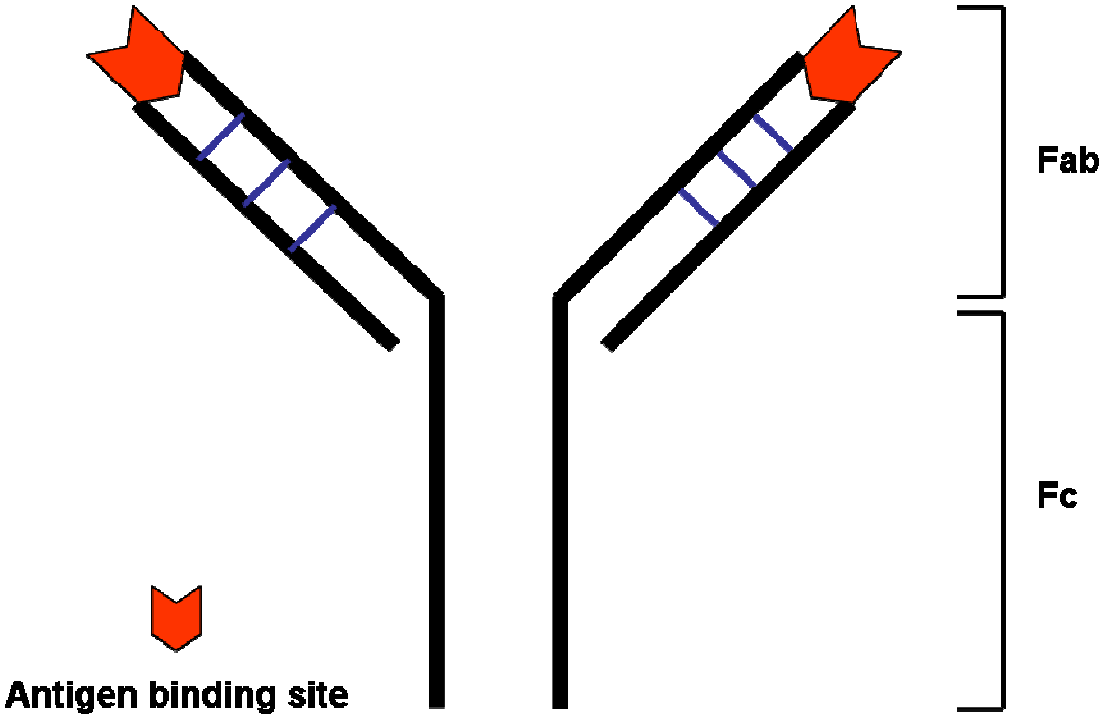

Figure 5. An immunoglobulin G (IgG) molecule showing the antigen binding site

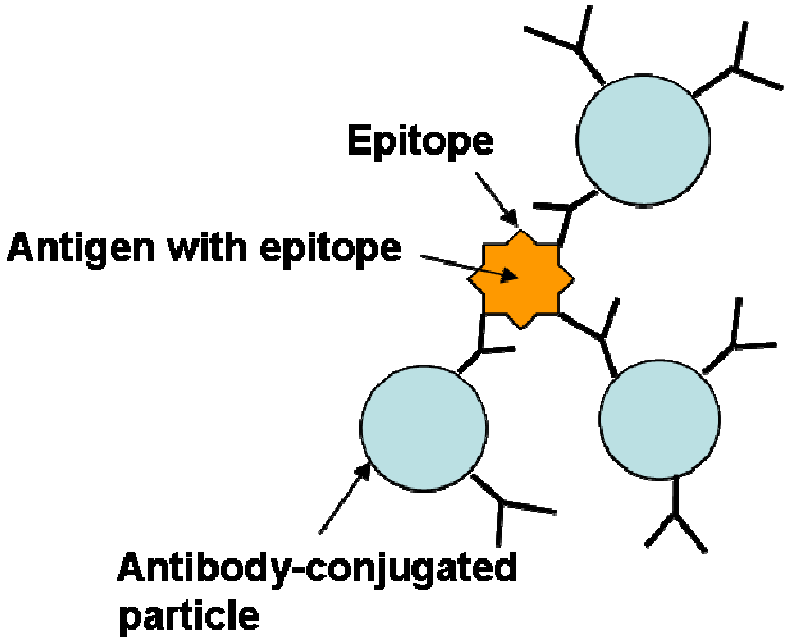

Figure 6. Schematic of particle immunoagglutination

PRESENT STUDY

The method, results, and conclusions of this study are presented in the paper appended to this dissertation. The following is a summary of the most important findings in this document.

To enhance the diffusional mixing of particle in a microfluidic device, plain polystyrene (PS) particle with SDS, PS particle with Tween 80, and highly carboxylated particle are tested. Particle agglutination with antibody-antigen reaction in a microfluidic device is presented visually by using image analysis. In addition, measured diffusivity of PS particle with SDS or Tween 80 and highly carboxylated particle as well as simulation of particle diffusion with numerical approach supports the results from image analysis. Highly carboxylated particle shows low non-specific binding and good diffusion in a microfluidic device.

To detect *E. coli* in a real time with very low detection limit, microfluidic detection system is developed. This system consists of a microfluidic device, micro-positioning device, and optical fiber. The use of proximity optical fibers around the view cell of a microfluidic device can quantify the light scattering of immunoagglutinated particles. The detection limit is less than 10 cfu ml^{-1} (0.1 cfu per device) without PBS washing (detecting viable, non-viable cells and free antigens), or less than 40 cfu ml^{-1} (4 cfu per device) with PBS washing (thus detecting viable cell only). This result is superior to other results of *E. coli* detection in a microfluidic device

To develop accurate microbial risk assessment in a water distribution system, microfluidic detection system is employed in a straight pipe injection system. *E. coli* is detected and its axial dispersion is monitored using microfluidic system. The detection limit is less than 10 cfu ml-*1*. To predict flow behavior of E. coli in a water distribution system, 2-D computational fluidic dynamics model is used. Microfludic detection system is appropriate for monitoring waterborne pathogens in a water distribution system. Further, The numerical simulation to predict flow behavior of *E. coli* is another key player for microbial risk assessment in a water distribution system together with detection.

REFERENCES

1. Bruus, H., *Theoretical Microfluidics*. 2008: Oxford. 1 pgs.

2. Tabeling, P., *Introduction to Microfluidics*. 2005: Oxford. 12 pgs.

3. Madou, M.J., Fundamentals of Microfabrication*: The Science of Miniaturization.* 2nd ed. 2002: CRC. 65 pgs.

4. Haverkorn von Rijsewijk H.C., Legierse, P.E.J., Thomas, G.E., *Manufacture of LaserVision video disks by a photopolymerization process*, Philips Tech. Rev., 1982, 40: p. 287-297.

5. Xia, Y., Whitesides, G.M., *Soft lithography*, Annu. Rev. Mater. Sci., 1998, 28: p. 153-184.

6. Zhao, X.-M., Xia, Y., Whitesides G.M., *Soft lithographic methods for nano-fabrication*, J. Mater. Chem., 1997, 7: p. 1069–74

7. Rogers, J.A., Bao, J., Raju, V.R., *Nonphotolithographic fabrication of organic transistors with micron feature sizes,* Appl. Phys. Lett., 1998, 72: p. 2716-2718.

8. Erhardt, M.K., Nuzzo, R.G., *Fabrication of Pt-Si Schottky diodes using soft lithography patterning and selective chemical vapor deposition,* Lanmuir, 1999, 15:

9. Gomez, F.A., *Biological Applications of Microfluidics, Wiley.* 3 pgs.

10. Takayama, S., McDonald, J.C., Ostuni, E., Liang, M.N., Kenis P.J.A., Ismagilov R.F., Whitesides G.M., *Patterning cells and their environments using multiple laminar fluid flows in capillary networks,* Proc Natl Acad Sci USA, 1999, 96: p. 5545-5548.

11. deMello A.J., *Control and detection of chemical reactions in microfluidic systems,* Nature, 2006, 442: p. 394-402.

12. Han, J.-H., Heinze B.C., Yoon, J.-Y, *Single cell level detection of Escherichia coli in microfluidic device,* Biosens. Bioelectron., 2008, 23: p. 1303-1306.

13. Jensen K.F., *Microreaction engineering is small better?,* Chem. Eng. Sci., 2001, 56: 293-303.

14. Davis, J.E., Eberwine, J.H., Hinkle, D.A., Marciano, P.G., Meaney, D.F., McIntosh, T.K., *Methodological considerations regarding single-cell gene expression profiling*

for brain injury, Neuchem. Res., 2004, 29: p. 1113-1121.

15. Fend F., Raffeld, M., *Laser capture microdissection in pathology,* J. Clin. Pathol., 2000, 53: p. 666-672.

16. Sia, S.K., Whitesides, G.M., *Microfluidic devices fabricated in poly(dimethylsiloxane) for biological studies*, Electrophoresis, 2003, 24: p. 3563-3576.

17. Wikipedia: *The free encyclopedia,* http://en.wikipedia.org/wiki/Immunoassay.

18. Price, C.p., Newman, D.J., *Principles and Practice of Immunoassay*, 1991, Stockton. 1-2 pgs.

19. Roitt, I.M., Brostoff, J., Male, D.K., *Immunology.* 6th ed. 2001: Edinburgh. 71-74 pgs.

20. ORTEGA-VINUESA, J.L., BASTOS-GONZÁLEZ, D., *A review of factors affecting the performances of latex agglutination tests***,** J. Biomater. Sci. Polymer Edn, 2001, 12(4): p. 379–408.

APPENDICES

APPENDIX A:

The Enhanced Diffusional Mixing for latex Immunoagglutination Assay in a Microfluidic Device

APPENDIX B:

Single Cell Level Detection of *Escherichia Coli* in Microfluidic Device

APPENDIX C:

Flow behaviour of *Escherichia coli* in a straight pipe as monitored by a microfluidic device

APPENDIX A

THE ENHANCED DIFFUSIONAL MIXING FOR LATEX IMMUNOAGGLUTINATION ASSAY IN A MICROFLUIDIC DEVICE

Jin-Hee Han, Kye-Seong Kim, Jeong-Yeol Yoon

Department of Agricultural and Biosystems Engineering

The University of Arizona, Tucson, Arizona, 85721-0038, U.S.A.

Published in Analytica Chimica Acta 584 (2007) 252–259.

Received 19 July 2006; received in revised form 11 November 2006; accepted 15 November 2006; available online 24 November 2006

Abstract

Latex immunoagglutination assay in a microfluidic device is expected to be even easier than its large-sized, commercialized counterpart. However, such demonstration has had a limited success due to the difficulties in mixing in a microfluidic device, especially for the microparticles used in latex immunoagglutination assay. The primary goal of this work is to improve diffusional mixing towards the successful latex immunoagglutination in a microfluidic devices without any non-specific binding. To this end, SDS (sodium dodecyl sulfate, an ionic surfactant) or Tween 80 (polyethylenesorbitol ester, a non-ionic surfactant) was added to the antibody-conjugated polystyrene (PS) microparticle suspension. These surfactant-added particle suspensions were mixed with the target antigen solution at the Y-junction of a microfluidic device. The immunoagglutination and the diffusion behavior were visually identified with an inverted light microscope. Both surfactants showed some problems such as non-specific binding (with SDS) or very poor diffusion (with Tween 80). As an alternative approach, therefore, highly carboxylated PS microparticles, where the surface is saturated with carboxyl-terminated side chains, were evaluated without using any surfactants. These particles showed very low non-specific binding comparable to that with Tween 80 and good diffusional mixing equivalent to that with SDS.

Keywords: Latex immunoagglutination assay; Diffusional mixing; Microfluidic device; Non-specific binding

1. Introduction

Latex immunoagglutination assay has been popular in medical diagnostics due to its simplicity. There is also growing interest in conducting multiple immunoassays in a microfluidic device for real-time, high-throughput assay. It is therefore logical to pursue latex immunoagglutination assay in a microfluidic device, but such a demonstration has had a limited success due to the mixing problem within microchannels. The characteristic flow within a microchannel shows very low Reynolds number, due to the extremely small effective channel dimension. This leads to the condition of strict laminar flow, where the mixing should depend solely on diffusion. However, due to the large size of the particles (1–10μm) and particularly their agglutinates used in latex immunoagglutination assays, the diffusivity will be limited, which makes diffusional mixing difficult.

Considering solely of mixing the solutions of low-molecularweight molecules within a microchannel (for biochemical sensing), the turbulent mixing has been demonstrated to be the most effective. Volpert et al. [1] and Lee et al. [2] suggested cross-channel micromixers, where the secondary channel creates the cross-flows perpendicular to the main to achieve turbulent mixing. Stroock et al. [3] developed herringbone chaotic mixer that could generate three-dimensional twisting flow in a microchannel. Likewise, MacIness [4] and MacIness et al. [5] demonstrated the creation of plugs to generate turbulence in a microchannel. Takhistov et al. [6] created vortices in a narrow microchannel under the electroosmotic flow by introducing a potential drop across the charged segment. Diffusional mixing, on the other hand, has been less popular than the turbulent mixing, because turbulent mixing can speed thermal and chemical transport beyond diffusional limits inherent in laminar flow, leading to rapid mixing [7]. Hatch et al. [8] suggested competitive diffusion of antigen and antibody molecules in a T-

junction microchannel.

Although extensively studied, the above approaches are not appropriate for conducting latex immunoagglutination assays in a microfluidic device. Since the latex particles and their agglutinates are much bigger than the molecules tested in the works mentioned above, turbulent mixing may not be effective for such demonstration. Turbulent flow is rather a hindrance for binding of microparticles [7]. In addition, the complicated fabrication required to create turbulence may cause other problems to the particle agglutination. The same problem persists in the diffusional mixing, since the diffusivity of microparticles is rather poor, which will be evaluated later in this paper.

In addition, there have been several works where nano- or micro-particles were tested within microchannels. Lettieri et al. [9] demonstrated the trapping of 1–6μm particles into a certain place of a microchannel by using bi-directional electroosmotic and pressure-driven flows. Malmstadt et al. [10] suggested the method of immobilizing 100 nm latex particles in a microchannel. However, both studies did not use the particles for latex immunoagglutination assay and did not address the mixing issue of particles in a microchannel. In short, the latex immunoagglutination in a microfluidic device with ideal mixing has not properly been demonstrated so far.

An alternative method to achieve diffusional mixing in a microfluidic device is proposed here. First, we evaluated the effects of surfactant towards the diffusional mixing of particles. Surfactants can be used to improve the diffusion of particles as well as to enhance antigen–antibody binding. Sodium dodecyl sulfate (SDS), which includes a sulfate group, is known to improve the sensitivity of latex immunoagglutination assay

[11]. The ionic portion, the sulfate group, of SDS is also known to enhance diffusivity of particles due to increased surface charge density [12]. However, that sulfate ionic portion may also cause some non-specific bindings leading to false-positive readings [13]. On the other hand, non-ionic surfactant such as Tween 80 (polyethylene sorbitol ester) has known to provide colloidal stability as well as suppression of non-specific bindings [14–16]. However, this surfactant cannot enhance diffusivity of particles in the liquid phase due to its relatively lower polarity than the ionic surfactants, such as SDS, which will be addressed later in this paper.

Thus, a method that can enhance the diffusivity of particles in aqueous medium and simultaneously prevent non-specific binding is needed. In our previous work [17] we identified the possibility that the highly carboxylated polystyrene (PS) particles could meet both requirements mentioned in the above. These highly carboxylated PS particles were made through copolymerizing styrene with methacrylic or acrylic acid (MAA or AA), leading to the hydrophobic PS core, and hairy, hydrophilic but non-ionic PMAA or PAA shell [18]. These hairy chains bound to the surface, containing carboxyl terminal groups at the end, behave similar to the surface-bound surfactant. This inherent binding of hairy, hydrophilic side-chains is expected to contribute to better diffusion of particles, maximizing the particle stability and diffusivity with no concern of critical micelle concentration. This enhanced mobility of particles can also improve antibody–antigen binding for agglutination.

The primary goal of this study is to improve diffusional mixing towards the successful latex immunoagglutination, without any non-specific binding, under the

aminar flow conditions of a microfluidic device. The other objective is to develop an immunosensing microfluidic device potentially useful for environmental pathogen monitoring. SDS or Tween 80 was added to the antibody-conjugated PS particles, which were mixed with the target antigen solutions in a Y-junction microfluidic device. Alternatively, highly carboxylated PS particles were also evaluated for the same type of experiments. The immunoagglutination and the mixing behavior were observed with an inverted light microscope. Diffusion coefficients of the particles, with or without surfactants, were evaluated with dynamic light scattering (DLS) [19].

2. Experimental

2.1. Latex particles, antibodies and surfactants

0.92 μm polystyrene (PS) particles (Spherotech Inc., Libertyville, IL) and 0.92 μm highly carboxylated PS (HCPS) particles (Bangs Laboratories, Fishers, IN) were conjugated with anti-mouse IgG (catalog number M8642; Sigma–Aldrich Co., St. Louis, MO) by physical adsorption. The parking area of HCPS was 10.3 $Å^2$ $group^{-1}$ (determined with conductometric titration by the manufacturer), which corresponds to *ca*. 10 carboxyl groups nm^{-2}, indicating the surface is fully saturated with carboxyl side chains [20,21]. The parking area of typical (weakly) carboxylated PS particles are 100–200 ° $Å^2$ $group^{-1}$ (*i.e.*, 0.5–1 carboxyl groups nm−2) [22]. Dilutions were made using 10mM phosphate buffered saline (PBS; pH 7.4; Sigma–Aldrich). For surfactant-based experiments, non-ionic Tween 80 (T80 hereafter; catalog number P8192; Sigma–Aldrich) and ionic SDS (catalog number 71725; Sigma–Aldrich) were used. These surfactants were added to the

PS particle suspension together with anti-mouse IgG. The final surfactant concentrations were 0.02% (w/v), consistent with other studies and the suggested value from the particle manufacturers [23,24]. Mixing was performed using an orbital shaker (DS 500; VWR International Inc., West Chester, PA) at 350 rpm for 2 h. Mixed solutions were incubated overnight at 4ºC, followed by centrifuging at 9.9 *g* for 15 min. Supernatants were removed and the pellets were resuspended into PBS using a sonicator. This centrifuging-resuspension procedure was repeated twice. Anti-mouse IgG concentrations were 4.8 $\mu g ml^{-1}$ initially, 1.8–2.1 $\mu g ml^{-1}$ in the supernatants after the first centrifugation, and <0.1 $\mu g ml^{-1}$ in the supernatants after the second centrifugation (all evaluated with the UV absorbance at 280 nm). Low concentrations of anti-mouse IgG in the supernatants after the second centrifugation indicate the stable conjugation of antibodies to the particles. The surface coverage of anti-mouse IgG on four different particles could be evaluated from this data using the equations known in the literature [22,23]: 59–62%. This indicates the similar surface coverage on the four different 0.92 µm particles used: PS, PS + T80, PS + SDS and HCPS, as well as the negligible amount of free anti-mouse IgG in the solution that may affect the immunoagglutination. For comparison purpose, 5.26 µm HCPS (parking area = 37.4 $Å^2$ $group^{-1}$; Bangs Laboratories) were also used with no surfactant [20–22]. The final concentration of particles was 0.031% (w/v). IgG from murine serum (29.5 $\mu g ml^{-1}$; mouse IgG; catalog number I5381; Sigma) was used as a positive control (target antigen). IgG from rabbit serum (29.5 $\mu g ml^{-1}$; rabbit IgG; catalog number I5006; Sigma) was used as a negative control. Target concentrations for both positive and negative controls, 29.5 $\mu g ml^{-1}$, were randomly chosen to be excess amount

over the given amount of anti-mouse IgG on the particles.

2.2. Fabrication of microfluidic devices

Microfluidic devices were fabricated using the standard soft lithography with PDMS molding technique [25]. SU-8 photoresist (Microchem Corp., Newton, MA) was spun onto a microscope glass slide, resulting in a uniform layer of SU-8. Thickness of this SU-8 layer was 100 μm as measured with a profilometer (Alpha Step 2000, Tencor Instruments, Reston, VA). The SU-8/glass substrate was soft-baked at 95 ◦C for 20 min, then exposed to the UV light (365 nm) with a mask, followed by the post-baking at 95ºC for 10 min. After these baking processes, the glass slide was developed away with developer (PM acetate, Microchem Corp.) generating a mold made solely out of SU-8. Once the mold was completed, liquid PDMS (polydimethyl siloxane; silicon elastomer kit Sylgard 184; Dow Corning Corp., Midland, MI) was mixed thoroughly with the curing agent at the ratio of 10:1 and poured over the mold. This PDMS gel was then placed in a vacuum desiccator for 20 min to remove air bubbles from the prepolymer mixture.

Once the PDMS gel was completely degassed, it was cured at 65ºC for 1 h. The PDMS was then peeled off carefully from the mold. The PDMS microchannel has the dimensions of 200 μm(width)×100 μm(depth) as measured by a profilometer (Alpha Step 2000). The layout of Y-shape microfluidic device is shown in Fig. 1(a). The PDMS was bonded with a cover glass slide using oxygen plasma asher (Plasma Preen Cleaner/Etcher, Terra Universal Inc.) with the power of 550W for 20 s. This plasma bonding procedure

made the PDMS hydrophilic, which should remain hydrophilic for at least 24 h up to a week [26]. Therefore we used the fabricated devices within 24 h. A needle was used for making a hole in the PDMS channel. It was then connected with Teflon tubing (0.79mm o.d.; Upchurch Scientific, Oak Harbor, WA). All fabrications were performed in a class 100 clean room environment.

2.3. Microfluidic immunoagglutination assays

A syringe pump (KD Scientific, Holliston, MA) was used for injecting the above solutions to the microchannel under atmospheric pressure. Two Teflon tubes (0.79 mm o.d.) connected two 250 μL gastight syringes (Hamilton Co., Reno, NV) to the top openings of the PDMS substrate. Anti-mouse IgG-conjugated particles were injected to the one inlet of Y-junction microchannel, while the solutions of mouse IgG (positive control) or rabbit IgG (negative control) was injected to the other inlet of the channel. The flow rate was maintained at 1 nL min^{-1} from the syringe pump. Therefore, the resulting flow rates should be 1 nL min^{-1} for each channel before mixing and 2 nL min^{-1} after mixing. The microfluidic device was placed on an inverted light microscope (Nikon Instruments Inc., Tokyo, Japan) to monitor the particle agglutination within a microchannel. The images were captured with 10× or 40× objective lens and CF digital image capturing system (Photometrics, Tucson, AZ), and analyzed with MetaVue software (Universal Imaging Corp., Downington, PA).

The distribution of particles was analyzed by determining the frequency of singlet, doublet and triplet-or-more based on relative area of each agglutinates in microscopic

images. The measurement of area was performed by using MetaVue software.

2.4. Simulation of particle diffusion in a microfluidic device

To simulate the particle diffusion in a microfluidic device, the diffusion coefficients of four different particles (PS, PS + T80, PS + SDS and HCPS) should be evaluated. Doppler electrophoretic light scattering system (Coulter Delsa 440; Coulter

Corp., Hialeah, FL) was used to evaluate the diffusion coefficients of the plain and highly carboxylated PS particles. SDS and Tween 80 were used at concentration of 0.02% (w/v). The diffusion of particle in a microfluidic device is schematically shown in Fig. 1(b). The concentration profile of the particles as a function of position (x, y, z) and time (t) was analyzed with the Fick's second law of diffusion [27]:

$$\frac{\partial c}{\partial t} = D\left(\frac{\partial^2 c}{\partial x^2} + \frac{\partial^2 c}{\partial y^2} + \frac{\partial^2 c}{\partial z^2}\right) \tag{1}$$

By spreading Gaussian method, this partial differential equation can be solved as a function of time for each diffusional step [28]:

$$c(x, y, z, t) = M_0\left(\frac{1}{4\pi Dt}\right)^{\frac{3}{2}} \exp\left(-\frac{x^2 + y^2 + z^2}{4Dt}\right) \tag{2}$$

where c is the concentration of particles, M_0 the initial mass of particles, D the diffusion coefficient, x, y and z are the location of a particle, and t is the time.

The flux of particle in y-direction is given by Fick's first law of diffusion [27]:

$$J = -D\frac{dc}{dy} \tag{3}$$

where J is the flux of particle.

The calculation of the concentration profile of particles and the *y*-directional (diffusional) flux was performed by using MATLAB version 7.1.0. The value of x was changed against the product of time and the constant flow velocity, 1.6 μms^{-1}. The value of z was fixed at 1 μm away from the bottom surface of the microchannel. The supplied amounts of the particles were fixed at 625 μg, that was introduced at $t = 0$ s in the form of particle suspension. The time was varied from 1 to 10 s with 0.5 s step.

3. Results and Discussion

3.1. Immunoagglutination within a microfluidic device

0.92 μm plain PS particles with or without surfactants (Tween 80 or SDS), or 0.92 μm highly carboxylated PS particles without surfactant, all conjugated with anti-mouse IgG, were mixed with the mouse IgG (positive control) or rabbit IgG (negative control) solutions in a Y-junction microfluidic device. Regardless of particle diffusion, which will be discussed in the next section, particles should agglutinate at the boundary between the two streams of particle suspension and the target solution. Fig. 2 shows the representative images for this immunoagglutination at the stream boundary within the Y-junction, from 2 to 4 different but reproducible experiments. With positive control, lots of large agglutinated clumps were observed for all four types of particles. With negative control, almost no clumps were found for PS + T80 and HCPS, indicating no substantial non-specific bindings with these particles. However, some small clumps were identified for PS and PS + SDS, indicating the agglutination from non-specific bindings.

By using an image analysis software (MetaVue), we have counted the number of

singlet, doublet, and triplet-or-more particles, and summarized the result in Table 1. Basically, we drew circles and ellipses to match the particles or its clumps on the image window of MetaVue software, obtained effective particle diameter, and compared with the given particle diameter, 0.92 μm.We have repeated this analysis 2–3 times over different images, and the total fraction of singlet, doublet, and triplet-or more particles were evaluated. With positive control, all four particles showed substantial number of doublet and triplet-or more particles, indicating good immunoagglutination. It seems HCPS shows the best immunoagglutination (lowest singlet and highest doublet fractions) from Fig. 2 and Table 1. However, it is difficult to say which one is better than the others, since the net number of particles is different from image to image. With negative control, PS and PS + SDS showed large number of doublets, which clearly indicates agglutination from non-specific bindings. From this observation, we can at least say PS + T80 and HCPS meet our need; good immunoagglutination and low non-specific binding.

In case of PS + T80, big clumps could be found with positive control, but not with negative control, indicating good agglutination with few non-specific binding. This is consistent with the previous study [13], and the fact that non-ionic surfactants such as Tween 20 or Tween 80 are frequently used in commercial particle immunoassay kits [23]. On the other hand, SDS caused significant non-specific bindings with negative control, which is consistent with the previous research with the sulfonated PS particles [13]. From this observation, HCPS can be considered as the best choice for the immunoagglutination in a microfluidic device.

3.2. Diffusional mixing at the Y-junction

The diffusional behaviors of PS, PS + T80, PS + SDS and HCPS were evaluated from the microscopic images, as shown in Fig. 3. At t = 0 s, there is a clear boundary between the two streams of particle suspension (anti-mouse IgG-conjugated) and the target solution (of mouse IgG) for all four particles. This boundary disappears at t = 10 s for PS + SDS and HCPS, and the particles were able to fill the entire channel, *i.e.*, complete diffusion across the channel. Since the two inlet channels have identical channel dimension, tubing length and flow rate (pumped from a single syringe pump), molecular diffusion is solely responsible for this channel filling. With repeated experiments, we were able to identify that about 10 s is required for PS + SDS and HCPS to fully diffuse to the other side of the channel. However, no visually identifiable diffusion was observed for PS and PS + T80 at t = 10 s. Even with extended experimental time (up to 5 min), both PS and PS + T80 failed to diffuse to the other side of channel (data not shown).

Therefore, Tween 80 is ineffective for diffusion than SDS and high carboxylation to PS particles, although it provided low non-specific binding. This result can be explained in terms of polarity. The anion of SDS makes the PS particles more diffusive as it increases the surface charge density, leading to the increased mobility of particles. In case of HCPS, graft copolymerization of acrylic acid (AA) to PS leads to surface-bound, hairy AA side-chains. This leads to the surface negative charge at pH 7.4 that also leads to the increased mobility of particles. This “permanently attached” surfactant may enhance the diffusion in more facilitated way than non-ionic thus no charged Tween 80,

leading to the same extent of diffusion as that with SDS. And because this ‘‘permanently attached surfactant’’ does not have sulfate group common in ionic surfactant, good agglutination with few non-specific binding could be observed with HCPS. This indicates HCPS is the optimum medium to perform latex immunoagglutination in a microfluidic device. And since PS showed neither good diffusion nor low non-specific binding, it is clear that the carboxyl groups provide the desired functions: good diffusion and low non-specific binding.

We have also increased the Tween 80 concentration up to 0.2% (w/v) and found that the extent of agglutination increased but there was no effect on diffusion (data not shown). This indicates that the addition of Tween 80 to HCPS may enhance the immunoagglutination but will not affect the diffusional behavior.

3.3. Further immunoagglutination study with HCPS in microfluidic device

Fig. 4 shows the size effect on the agglutination of HCPS; 0.92 and 5.26 μm. 5.26 μm particles tend to form bigger agglutinates (28% singlet, 28% doublet, 44% triplet-or-more), while 0.92 μm particles form mostly doublets (16% singlet, 53% doublet, 31% triplet-or-more). This size effect can be explained in terms of the mobility of particle, which is inversely correlated to the particle size [29]. It seems, therefore, the mobility of particles affects the extent of agglutination.

3.4. Simulation of particle diffusion in microfluidic device

Table 2 shows diffusion coefficients of PS, PS + T80, PS + SDS and HCPS at pH 7.4. Diffusion coefficient of HCPS was comparable to PS + SDS and much greater than

those of PS and PS + T80. It seems the low diffusion coefficients for PS and PS + T80 could not overcome the strict laminar flow condition in a given microfluidic device. These results corroborate saturated carboxylation to the PS particles will lead to similar degree of diffusion as adding SDS.

Using these diffusion coefficients 0.16 and 0.36 $\mu m^2\ s^{-1}$ of PS + T80 and HCPS, we were able to numerically simulate the concentration profile and the flux of these particles, as particles diffuse from the origin to other direction at t = 5 s. Here the flux is defined as the amount of particles moving across the unit area per time. The results are shown in Fig. 5. At t = 5 s, HCPS is expected to move up to 8 μm, while PS + T80 is virtually motionless. The maximum flux of HCPS and PS + T80 were 5.57×10^{-4} and $3.14\times10^{-9}\ \mu g\ s^{-1}\ \mu m^{-2}$, respectively.

Both figures show clear differences between PS + T80 (almost no diffusion to *y*-direction) and HCPS (much enhanced diffusion to *y*-direction). This indicates the overall diffusion of HCPS is greatly enhanced from the virtually no diffusion of PS + T80, although the difference in the diffusion coefficients is not that significant (0.16 and 0.47 $\mu m^2\ s^{-1}$).

These numerical simulation results provide another supporting evidence to the fact that the high carboxylation to PS particles sufficiently enhances the diffusion within microfluidic channels, in addition to the evidences from the microscopic images (Fig. 3).

4. Conclusion

Three issues were addressed for demonstrating latex immunoagglutination assay

in a microfluidic device: (1) efficient mixing of the sample and the reagent solutions within a microchannel, (2) preventing non-specific binding, and (3) developing a simple and inexpensive device. In our study, highly carboxylated PS microparticles were identified to meet all the above requirements; sufficient diffusional mixing towards good agglutination, with few non-specific binding.

Acknowledgement

The authors thank Dr. Srini Raghavan in Department of Materials Science and Engineering at the University of Arizona for discussion and help in Doppler electrophoretic light scattering. Mr. Lonnie J. Lucas in Department of Agricultural and Biosystems Engineering at the University of Arizona helped in preparing immunoagglutination assay. The authors are grateful to the University of Arizona for the cleanroom facility and subsequent equipment assistance. The funding for this research was provided by the U.S. National Science Foundation (NSF), Award no. EEC-0600855 and by the Faculty Small Grants Program from the University of Arizona Foundation and the Office of the Vice President for Research, Graduate Studies, and Economic Development.

Table 1

The total fraction of particles in singlet, doublet, and triplet-or-more from 2 to 3 images take at the Y-junction, as evaluated by MetaVue software

Particle type	With Positive control			With Negative control		
	Singlet (%)	Doublet (%)	Triple or More (%)	Singlet (%)	Doublet (%)	Triple or more (%)
PS	26	59	15	31	67	2
PS+T80	31	38	31	91	9	0
PS+SDS	30	33	37	29	52	19
HCPS	16	53	31	93	7	0

PS, plain particles without surfactant; PS+T80, plain particles with Tween 80; PS+SDS, plain particles with SDS; HCPS, highly carboxylated PS particles without surfactant. All particles were conjugated with anti-mouse IgG

Table 2 Diffusion coefficients of 0.92-μm particles at pH 7.4 as evaluated by DLS.

Particles	Diffusion Coefficient ($\mu m^2 \cdot s^{-1}$)
PS	0.17 ± 0.02
PS+T80	0.16 ± 0.02
PS+SDS	0.36 ± 0.04
HCPS	0.47 ± 0.05

PS plain PS particles without surfactant; PS + T80, plain PS particles with Tween 80; PS + SDS, plain PS particles with SDS; HCPS; highly carboxylated PS particles without surfactnat. All particles were conjugated with anti-mouse IgG.
Surfactant concnetration = 0.02% (w/v)

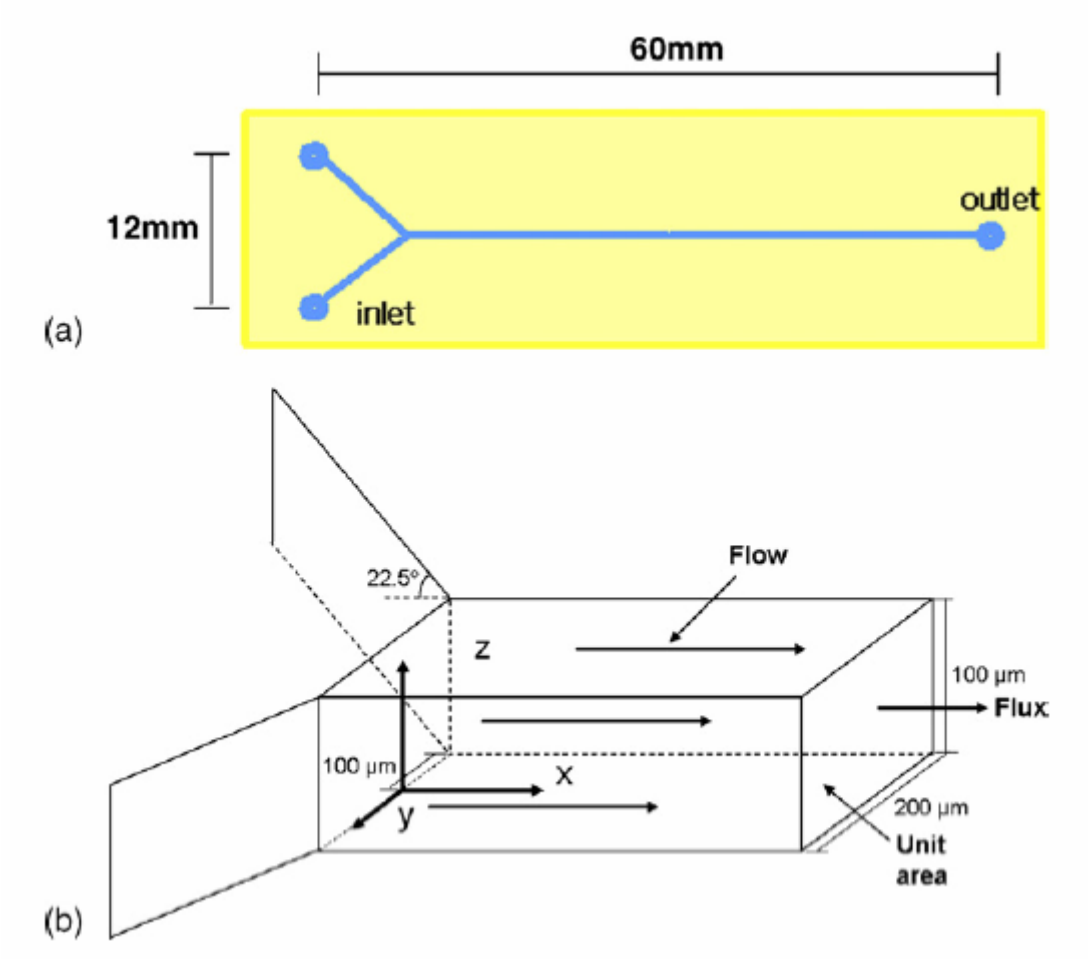

Fig. 1. (a) The layout of a microfluidic device, and (b) the schematic of particle diffusion in a microfluidic device.

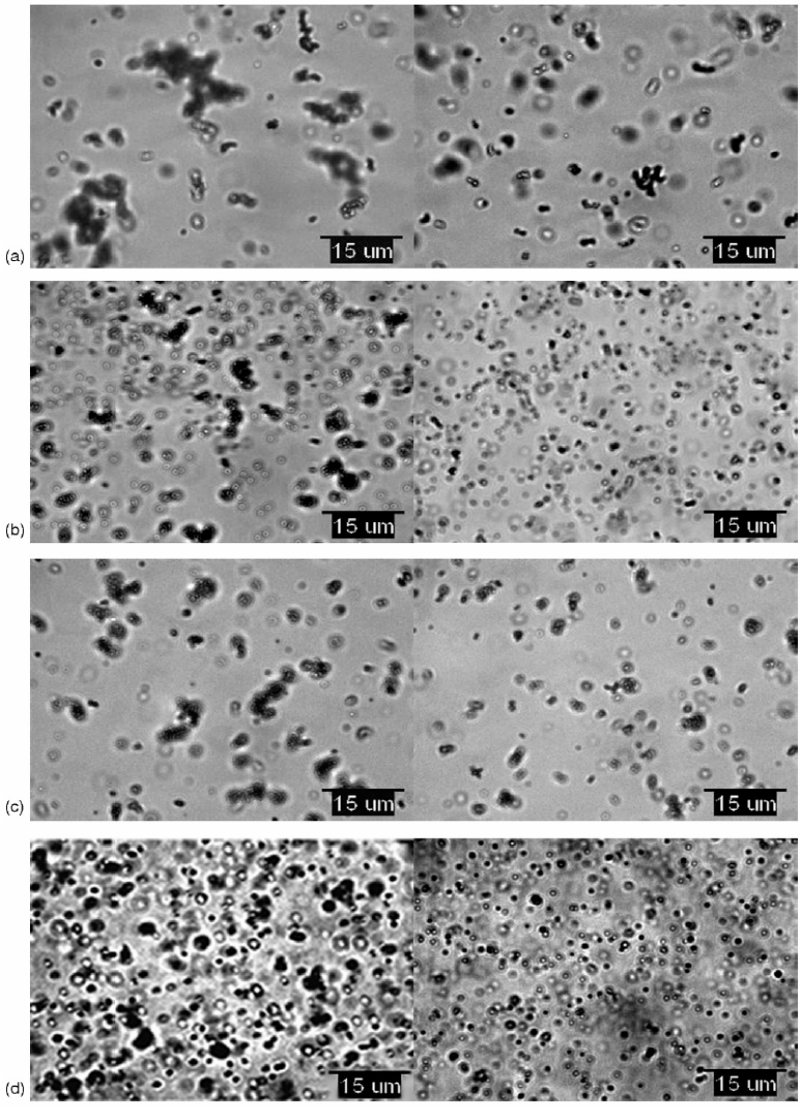

Fig. 2. The immunoagglutination of 0.92 μm anti-mouse IgG-conjugated particles (0.031%, w/v) with mouse IgG (29.5 $\mu g ml^{-1}$, positive control, left column) or rabbit IgG (29.5 $\mu g ml^{-1}$, negative control, right column) in a Y-junction microfluidic channel (3 min after initial injection): (a) plain PS particles without surfactant, (b) plain PS particles with Tween 80 (0.02%, w/v), (c) plain PS particles with SDS (0.02%, w/v), and (d) highly carboxylated PS particles (parking area = 10.3 $Å^2$ $group^{-1}$) without surfactant. All images were taken at the boundary of two streams near at the Y-junction.

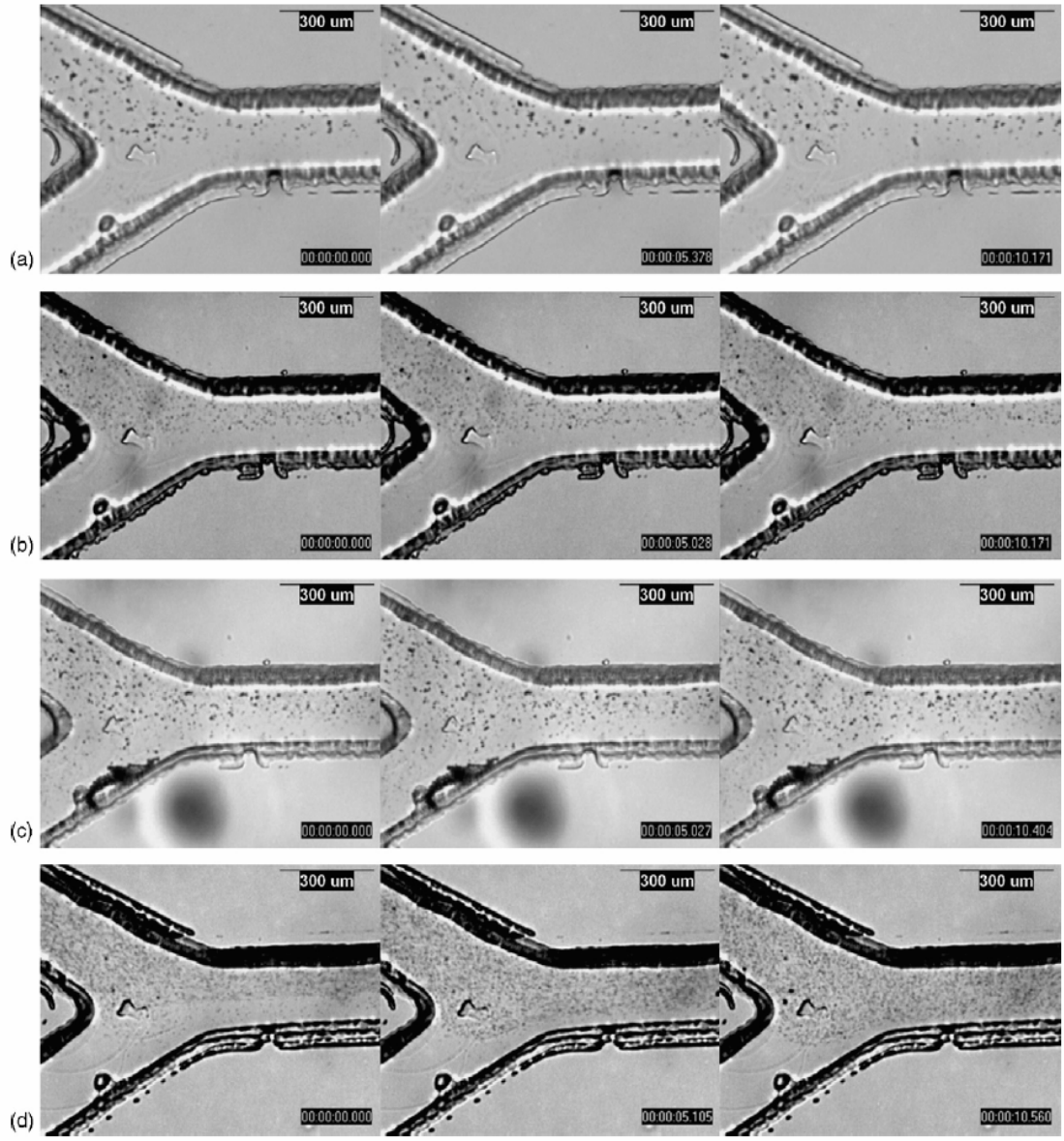

Fig. 3. The diffusion of 0.92 μm anti-mouse IgG-conjugated particles (0.125%, w/v) with mouse IgG (29.5 $\mu g ml^{-1}$, positive control) in a Y-junction microfluidic channel: (a) plain PS particles without surfactant, (b) plain PS particles with Tween 80 (0.02%, w/v), (c) plain PS particles with SDS (0.02%, w/v), and (d) highly carboxylated PS particles (parking area = 10.3 $Å^2$ $group^{-1}$) without surfactant. Images were taken at t = 0, 5 and 10 s.

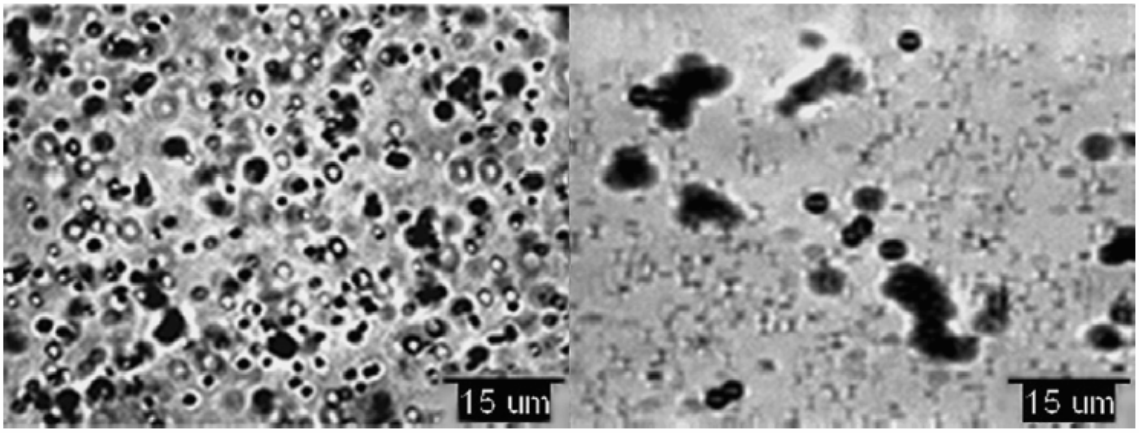

Fig. 4. Size effects to immunoagglutination of highly carboxylated PS particles: (a) 0.92 µm (singlet 16%, doublet 53%, triplet-or-more 31%) and (b) 5.26 µm (singlet 28%, doublet 28%, triplet-or-more 44%).

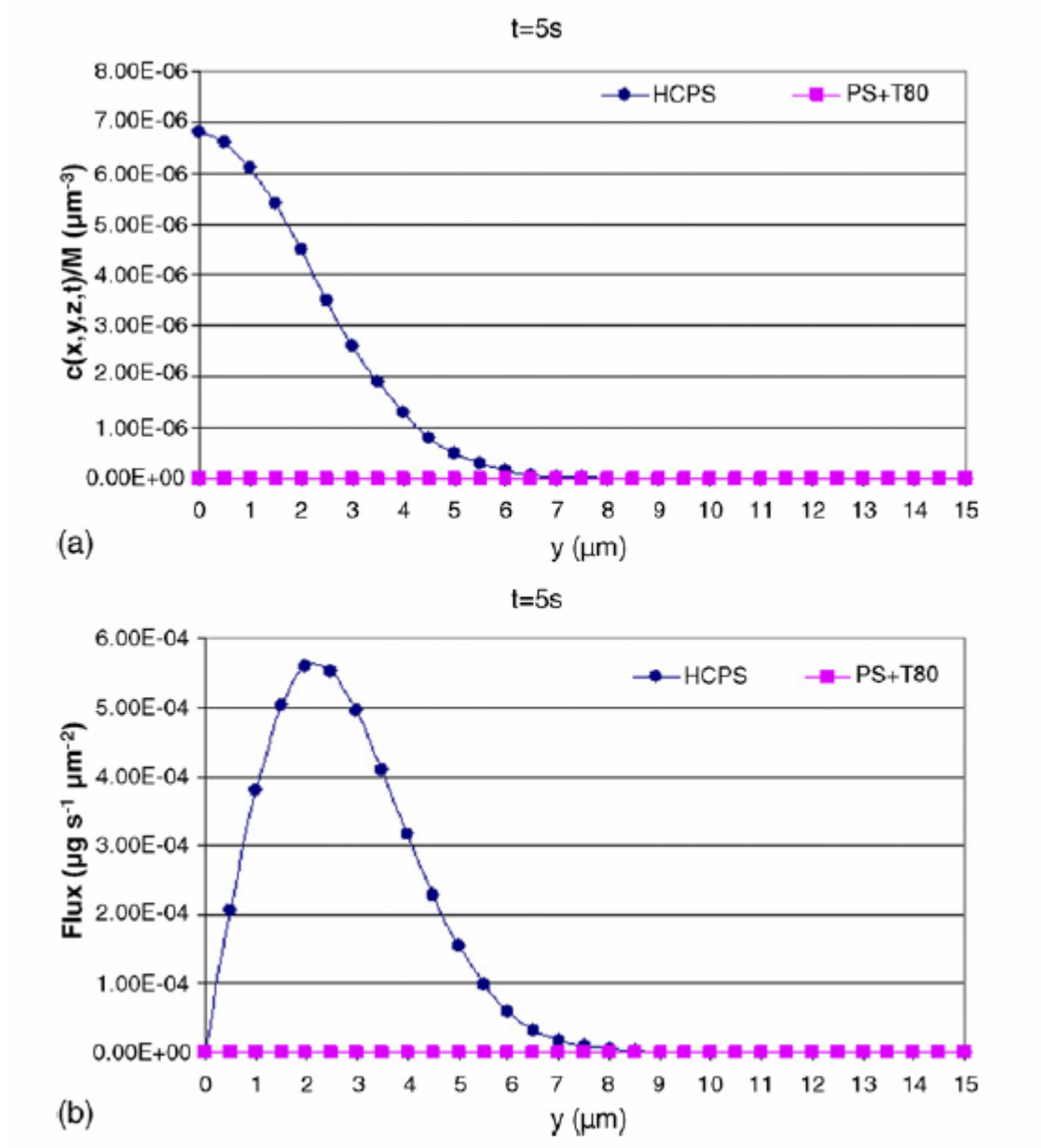

Fig. 5. (a) The concentration profile and (b) the flux of 0.92 µm highly carboxylated PS particles and the 0.92 µm plain PS particles with Tween 80, both conjugated with anti-mouse IgG, as a function of distance in *y*-direction, at $t = 5$ s.

References

[1] M. Volpert, I. Meizic, C. Meinhart, M. Dahleh, Proceedings of the ASME International Mech. Congress on Exposition, Nashville, TN, 1999, pp.483–487.

[2] Y.K. Lee, C. Shih, P. Tabeling, C.-M. Ho, Proceedings of the ASME International Mech. Congress on Exposition, Orlando, FL, 2000, pp. 505–511.

[3] A.D. Stroock, S.K.W. Dertinger, A. Ajdari, I. Mezic, H.A. Stone, G.M.Whitesides, Science 295 (2002) 647–651.

[4] J.M. MacIness, Chem. Eng. Sci. 57 (2002) 4539–4558.

[5] J.M. MacIness, X. Du, R.W.K. Allen, Phys. Fluids 15 (2003) 1992–2005.

[6] P. Takhistov, K. Duginova, H.-C. Chang, J. Colloid Interf. Sci. 263 (2003) 133–143.

[7] D.M. Holunga, R.C. Flagan, H.A. Atwater, Ind. Eng. Chem. Res. 44 (2005) 6332–6341.

[8] A. Hatch, A.E. Kamholz, K.R. Hawkins, M.S. Munson, E.A. Schilling, B.H. Weigl, P. Yager, Nat. Biotechnol. 19 (2001) 461–465.

[9] L. Lettieri, A. Dodge, G. Boer, N.F. De Rooji, E. Verpoorte, Lab Chip 3 (2003) 34–39.

[10] N. Malmstadt, S.Y. Wan, C. Shu, Y.T. Chew, Lab Chip 4 (2004) 412–415.

[11] Y. Kobayashi, N. Kohno, S. Wanibe, K. Hirayasu, H. Uemori, Y. Tagawa, T. Yokoyama, M. Shinagawa, Anal. Biochem. 348 (2006) 218–228.

[12] M.E. Ginn, in: E. Jungermann (Ed.), Cationic Surfactants, Dekker, New York, NY, 1970, pp. 353–372.

[13] J.-Y. Yoon, K.-H. Kim, S.-W. Choi, J.-H. Kim, W.-S. Kim, Colloids Surf. B 27 (2003) 3–9.

[14] L.B. Bangs, Pure Appl. Chem. 68 (1996) 1873–1879.

[15] H. Kawaguchi, in: T. Tsuruta, K. Kataoka, K. Ishihara, Y. Kimura (Eds.), Biomedical Applications of Polymeric Materials, CRC Press, Boca Raton, FL, 1993, pp. 299–324.

[16] J.A. Molina-Bol´ıvar, F. Galisteo-Gonzalez, R. Hidalgo-Alvarez, J. Immunol. Methods 211 (1998) 87–95.

[17] L.J. Lucas, J.-H. Han, J.-Y. Yoon, Colloids Surf. B 49 (2006) 106–111.

[18] G. Riess, C. Labbe, Macromol. Rapid Commun. 25 (2004) 401–435.

[19] J.C. Thomas, in: K.S. Schmitz (Ed.), Photon Correlation Spectroscopy: Technique and Instrumentation in Photon Correlation Spectroscopy Multi-Component Systems, SPIE Publications, 1991, pp. 2–18.

[20] J.-Y. Yoon, J.-H. Kim, W.-S. Kim, Colloids Surf. B 12 (1998) 15–22.

[21] J.-Y. Yoon, J.-H. Kim, W.-S. Kim, Colloids Surf. A 153 (1999) 413–419.

[22] L.B. Bangs, Handling-Specific Technotes No. 205: Adsorption to Microspheres, Bangs Laboratories Inc., Fishers, IN, 2002.

[23] L.B. Bangs, Handling-Specific Technotes No. 201: Adsorption to Microspheres, Bangs Laboratories Inc., Fishers, IN, 2002.

[24] E.P.K. Currie, J. van der Gucht, O.V. Borisov, M.A.C. Stuart, Pure Appl. Chem. 71 (1999) 1227–1241.

[25] Y. Xia, G. Whiteside, Annu. Rev. Mater. Sci. 28 (1998) 153–184.

[26] M.J. Owen, Aust. J. Chem. 58 (2005) 433–436.

[27] R.J. Hunter, in: L.R. White (Ed.), Foundations of Colloids Science, Oxford University Press, New York, NY, 1987, pp. 55–59.

[28] M.E. Glicksman, Diffusion in Solids: Field Theory, Solid-State Principles and Applications, John Wiley and Sons, New York, NY, 2000, pp. 59–70.

[29] Y.I. Aristov, I.S. Glaznev, A. Frenni, G. Restuccia, Chem. Eng. Sci. 61 (2006) 1453–1458.

APPENDIX B

SINGLE CELL LEVEL DETECTION OF *ESCHERICHIA COLI* IN MICROFLUIDIC DEVICE

Jin-Hee Han, Brian C. Heinze, Jeong-Yeol Yoon

Department of Agricultural and Biosystems Engineering

The University of Arizona, Tucson, Arizona, 85721-0038, U.S.A.

Published in Biosensors and Bioelectronics 23 (2008) 1303-1306.

Received 24 August 2007; received in revised form 21 November 2007; accepted 23 November 2007; available online 4 December 2007

Abstract

Detection of *Escherichia coli* K-12 in phosphate buffered saline (PBS) was demonstrated in a Y-channel polydimethylsiloxane (PDMS) microfluidic device through optical fiber monitoring of latex immunoagglutination. The latex immunoagglutination assay was performed for serially diluted *E. coli* solutions using 0.92-μm highly carboxylated polystyrene particles conjugated with polyclonal anti-*E. coli*. Pre-treatments such as cell lysis or culturing to enhance the signal were not used. Proximity optical fibers around the view cell of the device were used to quantify the increase in 45◦ forward light scattering of the immunoagglutinated particles. In order to reduce false positive signals caused by antibodies binding to non-viable *E. coli* cells or free antigens in solution, target solutions were washed three times, and then the results were compared to non-washing treatments. The detection limit was found to be less than 10 cfu ml^{-1} (1 cfu per device) without PBS washing (thus detecting non-viable cells and free antigens),or less than 40 cfu ml^{-1} (4 cfu per device) with PBS washing (thus detecting viable *E. coli* cells only).

Keywords: *Escherichia coli* K-12; Proximity optical fiber; Latex immunoagglutination assay; Latex agglutination test; Microfluidic device; Detection limit; Static light scattering

1. Introduction

Illnesses caused by waterborne pathogens range from mild gastrointestinal infections to life-threatening hemorrhagic colitis, haemolytic uremic syndrome, and thrombotic thrombocytopenic purpura (Hoffmann, 1993). Accidental outbreaks of waterborne pathogens have recently increased in drinking and irrigation water; consequently, a growing interest in developing more effective methods for detecting waterborne pathogens has arisen. Conventional detection methods prove to be time-consuming due to sample preparation and the need for pre-culturing samples, which make point-of-care and real-time detection very difficult. Nevertheless, several studies have been demonstrated in an attempt to overcome these complications. Muhammad-Tahir and Alocilja (2003) used a biosensor to detect *Escherichia coli* O157:H7 based on electrochemical sandwich immunoassay. Their detection limit was 7.8×10 cfu ml^{-1}. Yang and Li (2006) demonstrated multiple detection of *E. coli* O157:H7 and *Salmonella* using magnetic bead-cell-quantum dot complex on a glass slide, with detection limit of 10^4 cfu ml^{-1}. Mao et al. (2006) detected *E. coli* O157:H7 using DNA probe specific to *E. coli* immobilized on the surface of quartz crystal microbalance (QCM) sensor, with detection limit of 2.67×10^2 cfu ml^{-1}. Lin et al. (2004) used colorimetric quantification for detecting color change from 80-nm gold nanoparticles upon immunoassay of *E. coli* O157:H7 in polydimethylsiloxane (PDMS) microfluidic device, with detection limit of 10 ng. Li and Su (2006) captured *E. coli* O157:H7 by immobilizing antibodies within a microfluidic device, followed by detection with a UV–vis spectrophotometer. All of the above work, however, still required a considerable amount of time (especially for cell lysing and/or

culturing) and their detection limits were still relatively high (>100 cfu ml^{-1}). Furthermore, complications arose due to the overestimation of *E. coli c*oncentrations. These overestimations stem from the typical use of anti-*E. coli* that detects not just viable cells but also dead cells and free antigens in solution, while comparing the signals with the calculated concentrations of the conventional cell culturing method units (cfu ml^{-1}) that detected only viable cells (Nocker and Camper, 2006). Therefore, a better method is needed to detect solely viable target bacteria or viruses, with greater sensitivity, and in a simpler way.

In this study, we report the use of "proximity" optical fibers (i.e. the fibers are in close contact but not touching the microfluidic device) to quantify increased light scattering due to latex immunoagglutination in a microfluidic device, with a detection limit lower (preferably at the level of single cell) than other traditional methods. We have previously demonstrated latex immunoagglutination assay in a microfluidic device by using highly carboxylated submicron particles with no surfactant (Han et al., 2007).

2. Materials and methods

2.1. Chemicals and reagent

The conjugation of antibody to microparticles was performed as described previously (Han et al., 2007). Briefly, 1 ml of 0.02% (w/v), 0.92-μm highly carboxylated polystyrene (HCPS) particles (10.3 $Å^2$ parking area per carboxyl surface group; Bangs Laboratories, Fishers, IN) were conjugated with 1ml of 1.023 $μgml^{-1}$, anti-*E. coli* (polyclonal antibody developed in rabbit; catalog number ab13626; Abcam, Cambridge,

MA) by physical adsorption, for 33% surface coverage of antibody to particles (Bangs, 1999).

E. coli K-12 lyophilized cell powder was purchased from Sigma–Aldrich (catalog number EC1). The lyophilized *E. coli* was cultured in brain heart infusion broth (Remel, Lenexa, KS) at 37ºC for 20 h. The grown cell culture of lyophilized *E. coli* K-12 was serially diluted with 10mM PBS (pH 7.4) by 10^{-5} to 10^{-8}. As the lyophilized powder of *E. coli* K-12 may contain dead cell fragments and free antigens, the diluted *E. coli* K-12 solutions were washed by centrifuging at 2000×*g* for 15 min, followed by elimination of supernatants and resuspension in PBS. This centrifugation–resuspension was repeated three times to ensure complete removal of dead cell fragments and free antigens. The viable cell count was performed by planting 200 µl dilutions to eosin methylene blue agar (DIFCO, Lawrence, KS), which was incubated again at 37ºC for 20 h. To stain viable and non-viable cells, SYTO 9 and propidium iodide (LIVE/DEAD BacLight Viability Kit; Invitrogen, Carlsbad, CA) were used following protocol as described in manufacturer's product information (Molecular Probes, 2004). Stained *E. coli* cells were observed with a fluorescent microscope (Nikon, Tokyo, Japan), followed by counting the cells using Petroff–Hausser counting chamber (Electron Microscopy Sciences, Hatifield, PA).

2.2. Fabrication of microfluidic device

Microfluidic devices were fabricated by standard soft lithography with the PDMS molding technique (Xia and Whitesides, 1998). The PDMS microchannel has the dimensions of 200 μm(width)×100 μm(depth) as measured by a profilometer (Alpha Step 2000, Tencor Instruments, Reston, VA). The layout of Y-shape microfluidic device is shown in Fig. 1. In our previous study (Lucas et al., 2007), a second PDMS slide was used as a cover in order to get a sufficient light path length (800 μm) in the view cell; however, this made it difficult to acquire strong light scattering signals. In this study, a hole was made (diameter = 2 mm; depth = 2 mm) through the PDMS channel using a hole puncher to produce a view cell. Glass slides were bound on both top and bottom sides of the view cell using oxygen plasma asher (Plasma Preen Cleaner/Etcher; Terra Universal, Fullerton, CA) at 550W for 20 s, as shown in Fig. 1 (middle). The plasma bonding procedure also made the PDMS hydrophilic, which remains hydrophilic from 24 h to 1 week (Owen, 2005). This modified layout produced a sufficient light path length, thus enhancing the signal much better than our previous method. Two inlets and one outlet were then connected to Teflon tubings (0.79 mm OD; Upchurch Scientific, Oak Harbor, WA).

2.3. Light scattering detection

The experimental setup for light scattering detection using a microfluidic device is schematically shown in Fig. 1 (top) and a photograph is available in Fig. 1 (bottom). The USB4000 miniature spectrometer, model LS LED light source, and fiber optic cables

(Ocean Optics, Dunedin, FL) are arranged in what is known as "proximity" fiber arrangement. This means that the fiber distal ends are both very close (1 mm) but not touching the microfluidic device. The two optical fibers for lighting and detection have a 600 μm core diameter and 30 μm cladding with optimal transmission in the UV–vis wavelengths. The fibers are 1.0m in length with SMA-905 connectors (probes) on each end. The numerical aperture of these optical fibers and probes is 0.22 with an acceptance angle of 25º. The 380 nm wavelength UV LED supplies 45 μW power to the optical fiber assembly. The second fiber is positioned as a detector above the chip at a 45º angle to measure light scattering while avoiding any of the direct incident light beam. To inject microparticles conjugated with anti-*E. coli* and *E. coli* target solutions to the Y-junction microchannel, a syringe pump (KD Scientific, Holliston, MA) was used. Two Teflon tubes (0.79 mm OD) connected two 250-μl gastight syringes (Hamilton, Reno, NV) to the top openings of the PDMS substrate.

For proof-of-concept experiments, two-well glass slides model 48333 (VWR, West Chester, PA) were also used (Fig. 1, left-top). These slides have two polished spherical depressions of 18 mm diameter and 800 μm depth, potentially leading to stronger signal.

3. Results and discussion

3.1. Viable vs. non-viable E. coli cells

Fig. 2 shows the fluorescent microscopic images of stained *E. coli* in PBS buffer at a 10^{-2} dilution, with or without washing (to remove dead cell fragments and free

antigens; refer to Section 2.2). *E. coli* in PBS without washing showed the viable to non-viable ratio of approximately 4:1 (2.62×10^7 viable cells ml^{-1}; 6.84×10^6 non-viable cells ml^{-1}) as shown in Fig. 2 (left). Non-viable cell counts do not account for free antigens, because the fluorescent dyes (SYTO 9 and propidium iodide) in the LIVE/DEAD BacLight Bacterial Viability Kit stain nucleic acids (DNA and RNA). The number of free antigens that can be recognized by anti-*E. coli* would be substantially higher than the non-viable cell counts. The *E. coli* in PBS with washing showed a ratio of 100:1 (1.71×10^7 viable cells ml^{-1}; 1.71×10^5 nonviable cells ml^{-1}), showing *E. coli* cells are mostly viable (Fig. 2, right). The three times washing procedure enables the number of viable cells to be maintained while eliminating almost all non-viable cells.

3.2. Detection of E. coli using proximity optical fibers

Fig. 3 shows the light scattering signals for *E. coli* K-12 in PBS, with or without washing, in two different setups; namely, two-well glass slide or microfluidic device. A total of four different dilutions were made: 10^{-5}, 10^{-6}, 10^{-7}, and 10^{-8}, thus making standard curves. PBS buffer was used as a negative control (blank). The presented light intensity signals in the standard curves were subtracted by blank signal, which includes no analyte. The data is comprised of the averages of five different experiments. The detection limit was determined by performing *t*-tests between the blanks and each dilution. The results in Fig. 3 indicate a significant difference between each dilution and the blank ($p < 0.05$). The detection limit for *E. coli* in PBS buffer without washing was 9.1 cfu ml^{-1}. This detection limit is equivalent to <1 cfu per device considering the

control volume (0.1 ml) of a microfluidic device. This remarkable sensitivity level may be overestimated, as we know from Section 3.1 that there may exist a considerable number of dead *E. coli* without washing, subsequently releasing even more free antigens. These dead cells and free antigens also bind to anti-*E. coli* causing agglutination and increasing light scattering signal while not contributing to the number of colonies represented in cfu ml^{-1} unit (Nocker and Camper, 2006). The filled symbols in Fig. 3 show the results with washing, i.e. three times centrifuging and resuspending the *E. coli* culture, which eliminated dead cells and free antigens. This time, detection limit was 40 cfu ml^{-1} or 4 cfu per device. Although this detection limit is higher than those without washing, this level of sensitivity is greatly superior to the other detections performed in a microfluidic device. Both standard curves for two-well slide and microfluidic device showed linearity with changing concentration of *E. coli*, although the light intensity using two-well slide was stronger than that using microfluidic device. Through these calibration curves, partially quantification of specific concentration of *E. coli* K-12 can be available in the range of $0–10^4$ cfu ml^{-1}.

4. Conclusion

We demonstrated the real-time detection of *E. coli* through latex immunoagglutination using a microfluidic device with proximity optical fibers. This method is essentially one-step and requires no sample pre-treatment or cell culturing. The detection limit was as low as 40 cfu ml^{-1} or 4 cfu per device (viable cells only), or <10 cfu ml^{-1} or <1 cfu per device (including dead cells and free antigens), which are superior

to the other results of the *E. coli* detection performed in a microfluidic device. For further research, (1) using higher concentration of target over 10^4 cfu ml^{-1} to determine entire sensing range of our detecting system, (2) testing reusability of a microfluidic device to maintain consistent signal reading with varying concentration of target, (3) improving signal-to-noise ratio (SNR) to obtain perfect linearity in standard curve will be studied.

Acknowledgments

The authors are grateful to Dr. Lonnie J. Lucas at the University of Arizona (UA), currently at Aret´e Associates, for the help in optical fiber setup, and to Micro/Nanofabrication Center at UA for the clean room facility and subsequent equipment assistance. This work was funded by the U.S. National Science Foundation (NSF) award no. EEC-0600855 and National Veterinary Research and Quarantine Service (NVRQS), Republic of Korea, award no. C-AD14-2006-11-1. BCH also acknowledges the support from UA/NASA Space Grant undergraduate internship.

Appendix A. Supplementary data

Supplementary data associated with this article can be found in the online version, at doi: 10.1016/j.bios.2007.11.013.

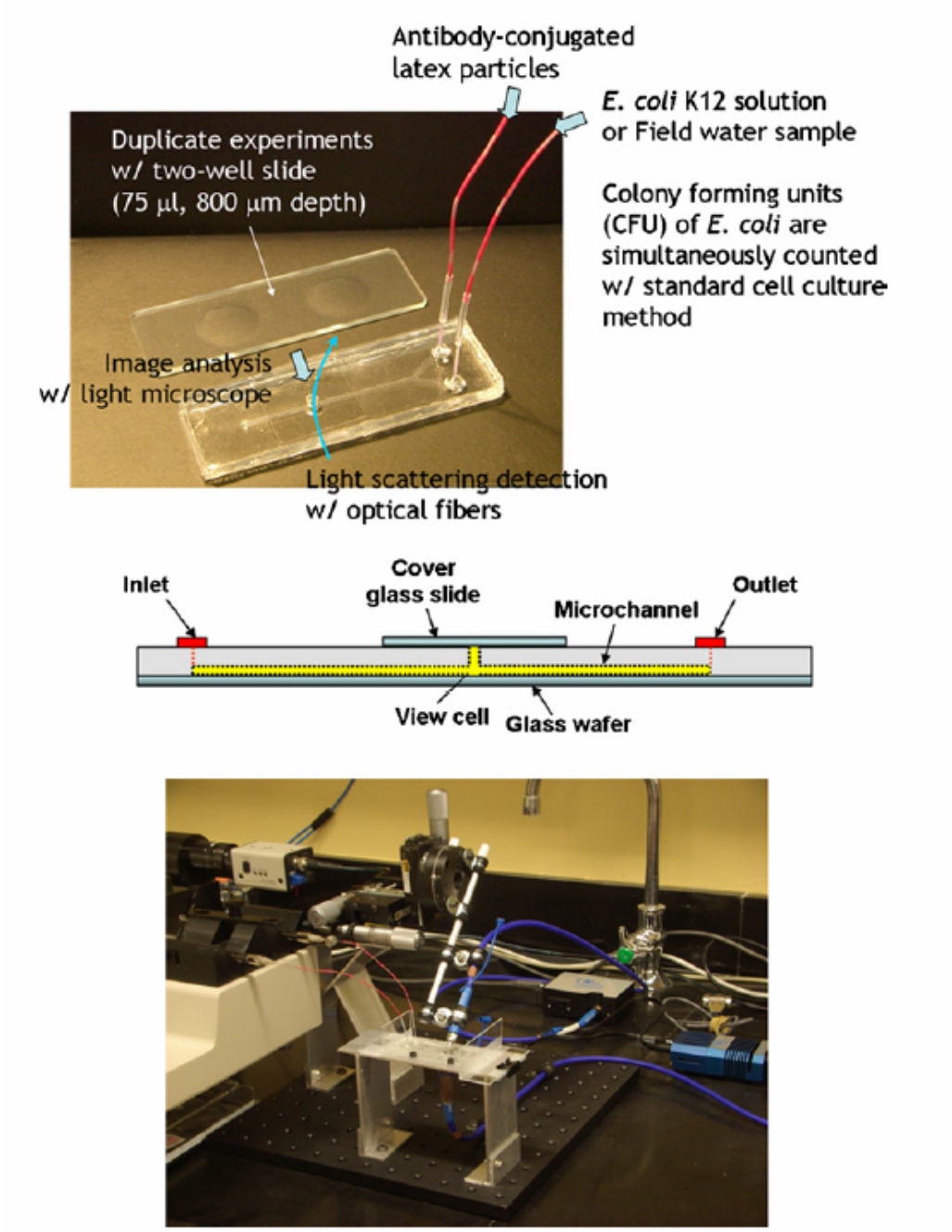

Fig. 1. Top: a two-well slide and a Y-shape microfluidic device with the schematic illustration for the experimental procedure. Middle: the slide view of a microfluidic device. Bottom: a microfluidic device and proximity optical fibers with a portable spectrometer and a UV (380 nm) light source, for optical fiber detection.

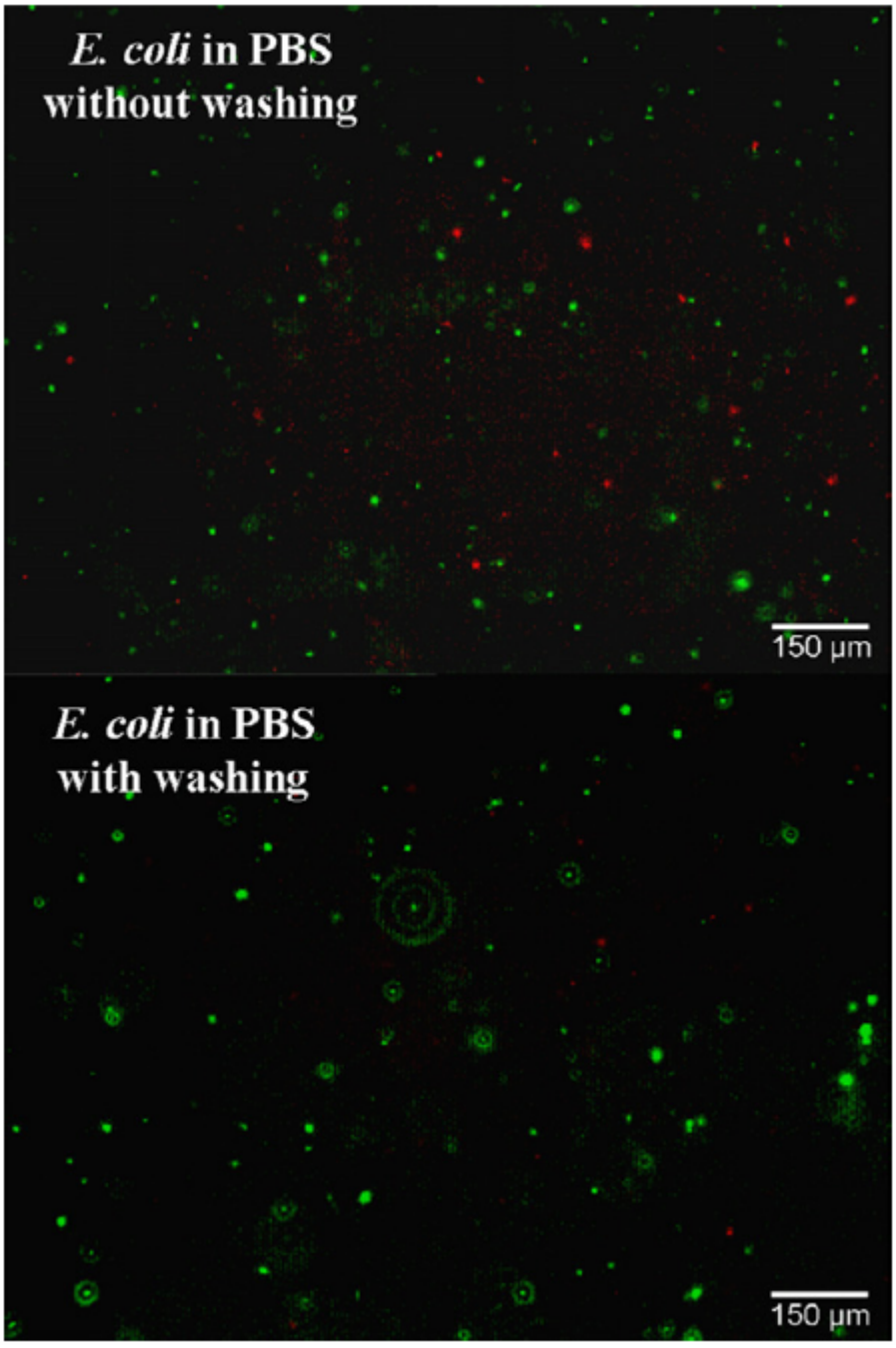

Fig. 2. Fluorescent microscopic images of stained *E. coli* cells in phosphate buffered saline (PBS) without washing (top) and with washing (bottom).

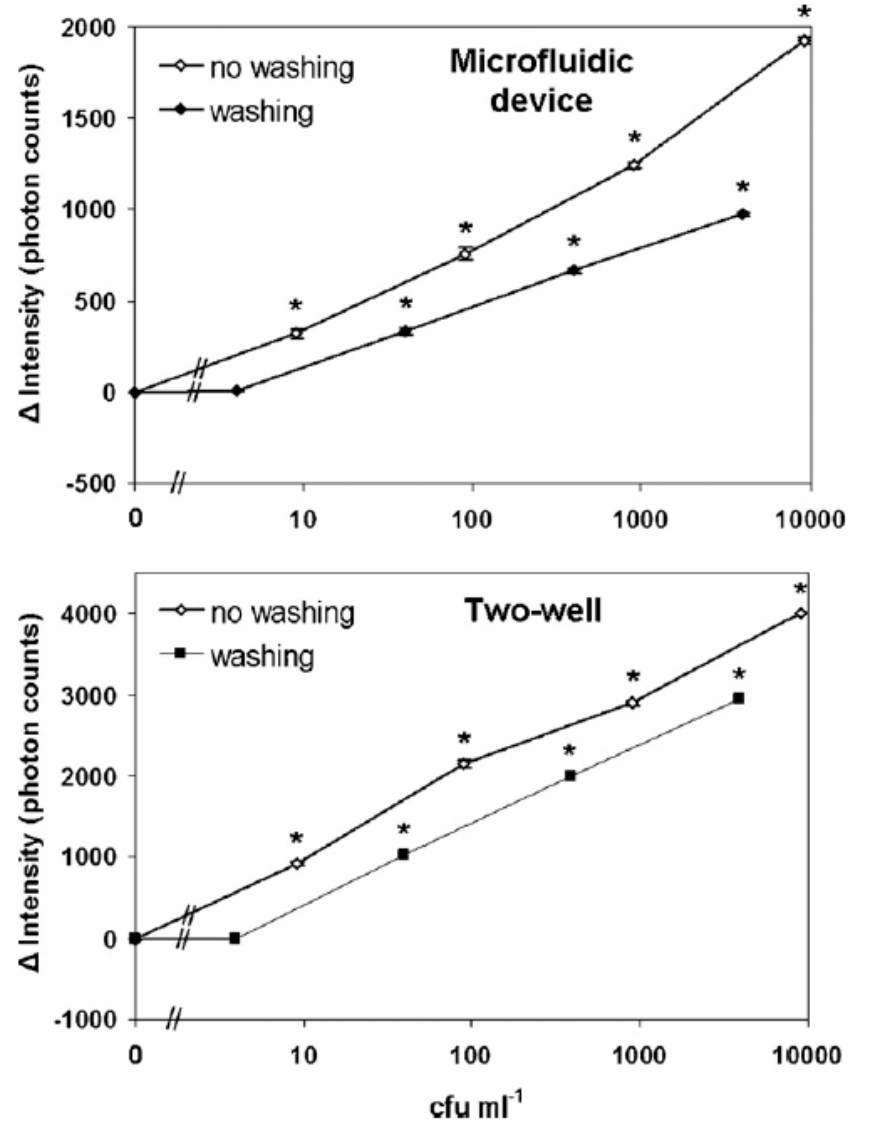

Fig. 3. Light scattering intensities of immunoagglutinated *E. coli* K-12 solutions in phosphate buffered saline (PBS) at various dilutions (10^{-5} to 10^{-8}). Anti-*E. coli* were conjugated at 33% surface coverage to 0.02% (w/v), 0.92-µm highly carboxylated polystyrene particles (parking area = 10.3 $Å^2$). Top: microfluidic device immunoassay. Bottom: two-well slide immunoassay. All data are the intensity difference of scattered light with and without analyte. Error bars are standard deviation. *represents significant difference from blank signal.

References

Bangs, L., 1999. TechNote #204: Adsorption to Microspheres. Bangs Laboratories, Fishers, IN, http://www.bangslabs.com.

Han, J.-H., Kim, K.-S., Yoon, J.-Y., 2007. Anal. Chim. Acta 584, 252–259.

Hoffmann, S.L., 1993. Am. J. Med. Sci. 306, 398–406.

Li, Y., Su, X.-L., 2006. J. Rapid Method Autom. Microbiol. 14, 96–109.

Lin, F.Y.H., Sherman, P.M., Li, D., 2004. Biomed. Microdevices 6, 125–130.

Lucas, L.J., Chesler, J.N., Yoon, J.-Y., 2007. Biosens. Bioelectron. 23, 675–681.

Mao, X., Yang, L., Su, X.-L., Li, Y., 2006. Biosens. Bioelectron. 21, 1185–1778.

Molecular Probes, 2004. LIVE/DEAD BacLight Bacterial Viability Kits. Molecular Probes, Eugene, OR, http://www.probes.com.

Muhammad-Tahir, Z., Alocilja, E.C., 2003. IEEE Sens. J. 3, 345–351.

Nocker, A., Camper, A.H., 2006. Appl. Environ. Microbiol. 72, 1997–2004.

Owen, M.J., 2005. Aust. J. Chem. 58, 433–436.

Xia, Y., Whitesides, G.M., 1998. Annu. Rev. Mater. Sci. 28, 153–184.

Yang, L., Li, Y., 2006. Analyst 131, 394–401.

APPENDIX C

FLOW BEHAVIOUR OF *ESCHERICHIA COLI* IN A STRAIGHT PIPE AS MONITORED BY A MICROFLUIDIC DEVICE

Jin-Hee Han, Jeong-Yeol Yoon*, Christopher Y. Choi, Melissa Bui, Ryan Sinclair

Department of Agricultural and Biosystems Engineering

The University of Arizona, Tucson, Arizona, 85721-0038, U.S.A.

.

Abstract

Accurate and real-time assessment of waterborne pathogens has been a critical issue for the safety of a water distribution system. Such ability is currently unavailable, making it impossible to predict the flow behaviour of pathogens in a water distribution system. Opto-microfluidic detection system (based on the light scattering from latex immunoagglutination assay) is utilized to detect *Escherichia coli* (model waterborne pathogen) in real time and with high sensitivity, for a straight pipe (model water distribution system). Water samples are collected downstream of a straight pipe with an automatic sampler and analyzed with the microfluidic system, which cell fragments and free antigens as well. Assay time is <5 min per assay and detection limit is 10 cfu ml^{-1}. For comparison purpose, viable *E. coli* cells are counted with conventional culturing method (assay time is more than a day). Salt tracer is also tested by measuring electric conductivity. Laminar (Re = 1102) and turbulent (Re = 6144) flows are used in a pipe. Axial dispersion is observed for cell fragments and free antigens (from *E. coli*), similar to salt, but not for viable *E. coli* cells in laminar flow. No axial dispersion is observed for all three targets in turbulent flow. Based on this observation, we simulate flow behavior of *E. coli* in s straight pipe flow using a 2-D computational fluid dynamics (CFD) model and EPANET. The CFD model shows reasonably good agreement to the experimental data.

Keywords: *Esherichia coli*; Latex immunoagglutination; Water distribution system; Axial dispersion; Light scattering; Microfluidic device, Computational fluid dynamics; EPANET.

1. Introduction

Pathogenic contamination is one of the most serious problems affecting the safety of drinking and irrigation water. Contrary to common belief, water supply system may be vulnerable to not only accidental or natural contamination, but also deliberate contamination with pathogenic agents (the latter can be considered as an act of terrorism). These pathogens should be detected in the early stage of systemic contamination, which requires an accurate and real-time risk assessment of biological agents. This type of risk assessment requires a fully automated and portable. Since we do not have such a sensor system, the transport behaviour of pathogenic agents has not been predicted accurately in a water distribution system.

Although several microfluidic-based methods have been attempted for detecting waterborne pathogens in laboratory studies, none have investigated macro-flow or water distribution systems. The following advantages are expected for these methods, as compared to conventional laboratory-based methods: faster and multiplexed detection, lesser consumption of reagents, and smaller equipment size/weight. Lin et al. (2004) reported the detection method of *Escherichia coli* O157:H7 using colorimetric immunoassay in a polydimethylsiloxane (PDMS) microfluidic device (detection limit: 10 ng, equivalent to 3×10^4 cells). Li and Su (2006) captured *E. coli* O157:H7 with the

antibodies immobilized in a microfluidic device, followed by detection with a UV-visible spectrometer (detection limit: $10\text{-}10^2$ cfu ml^{-1}). Recently, Han et al. (2008) detected viable and/or non-viable *E. coli* in real time through light scattering of latex immunoagglutination in a microfluidic device (detection limit: 40 cfu ml^{-1} for viable cells; <10 cfu ml^{-1} for viable and non-viable cells). We attempt to use this microfluidic-based system for real-time detection of waterborne pathogens in a water distribution system (a straight pipe in this work). By doing so, we attempt to predict the flow behaviour of waterborne pathogens in a model water distribution system that has been neither predicted nor experimentally evaluated.

The flow behavior in pipe(s) has been investigated since 1950's. Taylor (1953, 1954) analyzed the dispersion of salt injected into a circular capillary tube in which water was flowing. His axial dispersion model was valid when the dimensionless time ($T = 4D \cdot t / d^2$; D = molecular diffusion coefficient; d = the inner diameter of a pipe, t = elapsed time) was higher than 0.7 and Peclet number ($Pe = a \cdot u_{\max} / D$; a = the radius of a pipe, $u_{\max}$ = the maximum velocity) was higher than 500. When a salt tracer is injected into a pipe as an ideal pulse, the concentration profile of a salt tracer can be constructed over time at the downstream that is typically bell-shaped peak. Taylor showed that this concentration profile is symmetric in laminar flow. Later, Shankar and Lenhoff (1989) identified the concentration profiles of the tracer in a short pipe can be asymmetric due to the combined effects of axial convection, radial diffusion and axial diffusion. Numerical models have recently been developed using a computational fluid dynamic (CFD) methodology to predict mass transport of a foreign substrate in a pipe flow (Stovin et al.,

1997, Hancu et al., 2002; Ekambara and Joshi, 2004; Khalizov et al., 2006; Wilkening and Baraldi, 2007). These previous studies showed significant efforts of simulating complex transport phenomena of foreign substrates with CFD-based methods, in both laminar and turbulent flows. Axial dispersion is still a very difficult phenomenon to estimate in a real water distribution system because it varies as a function of Reynolds number, initial dispersion condition, and pipe length. In addition, all of the previous studies are based on a non-biological tracer (i.e. salt) and subsequent experimental measurement of electrical conductivity. Neither numerical modelling nor experimental verification was attempted for the biological agents (such as waterborne pathogens) in a pipe.

The first objective of our study is to develop a real-time microfluidic system for detecting *E. coli* in pipe flows. Our central hypothesis is that light scattering detection of latex immunoagglutination assay in a microfluidic device can detect *E. coli* at very low detection limit. We monitor *E. coli* concentrations against time, for the eluted fractions from laminar or turbulent flows in a straight pipe. The Second objective is to compare the flow characteristics of *E. coli* obtained by this opto-microfluidic detection with those of salt tracer (measured through electrical conductivity) and the results of conventional *E. coli* cell counting (not real-time) to identify differences between biological and non-biological agents in a pipe flow. The final objective is to simulate concentration profiles of *E. coli* in both laminar and turbulent flow by employing two-dimensional CFD models and to compare modelling outcomes with experimental data. The numerical simulation to predict flow behavior of *E. coli* is another key player for microbial risk assessment in a

water distribution system together with detection. For comparison purpose, the results from EPANET are used using same boundary conditions with CFD models.

2. Materials and methods

2.1. Antibody conjugation to microparticles

Antibody to *E. coli* (anti-*E. coli*) was conjugated to microparticles as described in Han et al. (2007). Briefly, 1 ml of 0.02% w/v, 0.92-μm highly carboxylated polystyrene particles (parking area = 10.3 $Å^2$ per carboxyl surface group; Bangs Laboratories, Fishers, IN, USA) were conjugated with 1 ml of 1.023 μg mL^{-1}, anti-*E. coli* solution (polyclonal antibody developed in rabbit; catalog number ab13626; Abcam, Cambridge, MA, USA) by physical adsorption, for 33% surface coverage of antibodies to the particles (Bangs, 1999).

These highly carboxylated particles should be mixed faster with target solution through their higher diffusivity, without using any surfactant. These particles make the latex immunoagglutination assay possible in microfluidic platforms, as we have recently demonstrated (Han et al., 2007). Free antibodies were washed by centrifuging the antibody-particle suspension twice, until no antibodies could be found in the supernatants (confirmed with the absorbance measurements at 280 nm).

2.2. E. coli preparation and its "conventional" assay

E. coli (ATCC 15597) was cultured in trypicase soy broth (TSB; DIFCO Scientific, Lawrence, KS, USA) at 37ºC for 12 h. The strain of *E. coli* grew fully to

stationary phase. Grown *E. coli* culture was diluted with dechlorinated tap water by 10^{-3}. The number of viable cells was counted by planting 10 µl of diluted samples to tryptic soy agar (TSA; DIFCO Scientific), followed by incubation at 37ºC for 18 h. To count viable and non-viable cells, 0.2 ml of 0.1% acridine orange was added to 2 ml of diluted *E. coli* samples. *E. coli* cells with green fluorescence were counted as viable in the images of fluorescent microscope images.

2.3. Fabrication of a microfluidic device

Microfluidic devices were fabricated by standard soft lithography with the poly(dimethyl siloxane) (PDMS) molding technique (Xia and Whitesides, 1998). Each PDMS microchannel was 200 µm wide and 100 µm deep, as measured by a profilometer (Alpha Step 2000, Tenco instruments, San Jose, CA, USA). The layout of a Y channel microfluidic device is shown in Fig. 1. We made a hole (diameter = 2 mm; depth = 2 mm) through a PDMS channel using a hole puncher to make a view cell. Two cover glass slides were bonded to the top and bottom slides of a view cell using oxygen plasma asher (Plasma Preen Cleaner/Etcher; Terra Universal, Fullerton, CA, USA) at 550 W for 20 s. Two inlets and one outlet (Fig. 1) were then connected to Teflon tubings (0.79 mm OD; Upchurch Scientific, Oak Harbor, WA, USA).

2.4. Optical detection on a microfluidic device

The experimental setup for light scattering detection using a microfluidic device is shown in Fig. 2. The USB4000 miniature spectrometer, model LS LED light source (45 µW) and fiber optic cables (all from Ocean Optics, Dunedin, FL, USA)

were arranged in what is known as “proximity” fiber arrangement. Details can be found in our previous study (Han et al., 2008), although the current setup is significantly improved version from the one in Han et al., 2008. Briefly, two optical fibers (core diameter = 600 μm; cladding = 30 μm; length = 1.0 m) were used for lighting and detection; One for delivering 380-nm light from the LED light source positioned underneath the microfluidic device, and the other to collect light scattering from the device positioned at 45° to avoid direct incident light. A syringe pump (KD Scientific, Holliston, MA, USA) was used to inject anti-*E. coli* conjugated microparticles and *E. coli* target solutions into the Y-junction microchannels.

2.5. Injection of salt and E. coli into a pipe

A straight pipe made out of poly(vinyl chloride) (PVC; length = 10 m; inner diameter = 16 mm) was used for the pipe injection experiments as shown in Fig. 3. Dechlorinated tap water was injected from a reservoir tank into the system by a centrifugal pump (SFBM 04876, Goulds Pumps, Seneca Falls, NY, USA) at 175 psi. The salt tracer (≥99.5%; 5 g l^{-1}; Sodium chloride; Sigma-Aldrich Co., St. Louis, MO), was then injected into the system at 50 ml min^{-1} with 10 s pulse using a micro injection peristaltic pump (75225-12, IDEX Corp., Vancouver, WA, USA). The flow rate was controlled by a valve (F800B, Parker Hydraulic Valve Division, Marysville, OH, USA) at the downstream end of a pipe. Electrical conductivity was measured to quantify the salt amount at both upstream and downstream ends of a pipe (length between upstream and downstream end = 7.84 m) using conductivity meters (CDTX-

1202, Omega Engineering, Stamford, CT, USA). The concentration of a salt tracer was monitored in real time using a data acquisition system (CR3000, Campbell Scientific, Logan, UT, USA). A series of water samples from a pipe were collected using a fraction collector (Eldex Laboratory, Napa, CA, USA) at the downstream end of a pipe system. These samples were analyzed with opto-microfluidic system (real-time, section 2.4) or conventional cell culturing (non-real-time, section 2.2) to determine *E. coli* concentrations. The automatic sampler was configured to take samples every 5 s for laminar flows and 1 s for turbulent flows.

2.6. CFD methodology

2.6.1. Governing equations

Unsteady state, incompressible laminar flow in a two dimensional pipe is solved using Navier-Stokes equations as follows (Kieffer et al., 2008):

$$\rho \frac{\partial u^i}{\partial t} = -\frac{\partial p}{\partial x^i} + \frac{\partial}{\partial x^j}\left[\mu\left(\frac{\partial u^i}{\partial x^j} + \frac{\partial u^j}{\partial x^i}\right)\right] - \left[\frac{\partial(\rho u^i u^j)}{\partial x^i} + \frac{\partial(\rho u^j u^i)}{\partial x^j}\right] \quad (1)$$

$$\frac{\partial u^i}{\partial x^i} = 0 \quad (2)$$

where the superscripts $i, j = 1, 2$ refer to the components in the x and y of the Cartesian coordinate system.

For the turbulent flow, standard $k-\varepsilon$ turbulent model were used. The turbulent kinetic energy k and its rate of dissipation ε are obtained from the following transport equations (Cebeci, 2003):

$$\frac{\partial}{\partial t}(\rho k)+\frac{\partial}{\partial x^i}(\rho k u^i)=\frac{\partial}{\partial x_j}\left[\left(\mu+\frac{\mu_t}{\sigma_k}\right)\frac{\partial k}{\partial x^j}\right]+G_k-\rho\varepsilon \tag{3}$$

$$\frac{\partial}{\partial t}(\rho k)+\frac{\partial}{\partial x^i}(\rho \varepsilon u^i)=\frac{\partial}{\partial x_j}\left[\left(\mu+\frac{\mu_t}{\sigma_\varepsilon}\right)\frac{\partial \varepsilon}{\partial x^j}\right]+C_{1\varepsilon}\frac{\varepsilon}{\kappa}G_k-C_{2\varepsilon}\rho\frac{\varepsilon^2}{k} \tag{4}$$

where the turbulent viscosity μ_t is obtained as:

$$\mu_t=\rho C_\mu\frac{\kappa^2}{\varepsilon} \tag{5}$$

The default values of constants are $C_{1\varepsilon}=1.44$, $C_{2\varepsilon}=1.92$, $C_\mu=0.09$, $\sigma_k=1.0$ and $\sigma_\varepsilon=1.3$.

For the transport of species in a flow, the conservation equation is used as follows (Lomax et al., 2003):

$$\frac{\partial}{\partial t}\left(\rho C\right)+\frac{\partial}{\partial x^i}\left(\rho u^i C\right)=-\frac{\partial}{\partial x^i}J+R \tag{6}$$

Equation (6) is simplified for the mass diffusion in laminar flow:

$$J=-\rho D\frac{\partial C}{\partial x^i} \tag{7}$$

For the mass diffusion in turbulent flow:

$$J=-(\rho D+\frac{\mu_t}{Sc_t})\frac{\partial C}{\partial x^i} \tag{8}$$

2.6.2. Boundary conditions

Simulations were performed using a commercial CFD package (FLUENT® 6.2 and GAMBIT® 2.2, FLUENT, Inc., Lebanon, NH, USA). The governing equations

were solved in an unsteady-state with first-order implicit. Species transport model was employed with the option of mixture species.

Fig. 4 shows an axis-symmetric geometry used in 2-D CFD simulations. Total length of a pipe (distance between upstream and downstream end, 7.84 m) was divided with five blocks to secure reasonable aspect ratio ($\frac{L}{r}$) for simulation. Simulations were performed one by one using each block which has geometry dimension of $r = 0.008 \times L = 1.6$ m (i.e. 100D). First, experimental concentration of species from upstream end was used as initial inlet condition. Modelling outcome at the outlet of one block was then used as inlet condition for next block. A quadrilateral mesh was defined with 4800 cells, of which 1600 cells (8×200) was used for the boundary layer region. A grid independent test was performed using 1600, 3200, 12000 cells. The modelling outcomes using these three cell size showed difference at maximum 1.6 % compared to the results using 4800 cells, which is acceptable (Hancu et al., 2002)

The types of inlet and outlet were set up as velocity inlet and pressure outlet, respectively. The flow velocity at inlet is determined by each Reynolds number (Re = 1102 or 6144). The gauge pressure was zero at outlet. The velocity and pressure parameters were linked and solved by SIMPLE algorithm (Ahmad and Lau, 2007).

In case of a turbulent flow, a turbulent intensity of 5% was used at inlet. The conditions of enhanced wall treatment and no slip were used on the wall boundary (Nallasamy, 1987). The Sc_t value used for the turbulent flow was determined by a

series of simulations at different values ranging from 0.01 to 2.0. Modelling outcome showed the best results at $Sc_t = 0.1$.

3. Results and discussion

3.1. Detection of E. coli

Table 1 shows the light scattering signals from an opto-microfluidic system and corresponding *E. coli* concentrations with conventional cell culture (hereafter "*E. coli* count") of the water samples collected from a straight pipe. Microfluidic signals are in real time (total assay time is less than 5 min each), while the *E. coli* counts are not (total assay time is more than a day). Fourteen samples were collected from a laminar flow (Re = 1,102), and eleven from a turbulent flow (Re = 6,144). Dechlorinated tap water is used as a negative control (i.e. blank signal, which is obtained my mixing the dechlorinated tap water to anti-*E. coli*-conjugated particle suspension). Each fraction is measured three times with an opto-microfluidic system, and their averages are shown in Table 1. Standard deviations are 0.1-4.2% for a laminar flow and 0.2-2.3% for the turbulent. The entire data set is a representative out of three data sets. Almost all fractions show significant differences in their microfluidic signals from that of blank ($p<0.05$), as indicated with *. Microfluidic signals show good match with *E. coli* counts (linearly proportional), indicating the linear range of light scattering assay in a microfluidic device is from 10 to 10^7 cfu ml^{-1}. Breakthrough is observed at 83 s for laminar flow, while at 21 s for turbulent flow, where *E. coli* concentration suddenly jumps up. A peak is observed at 113 s (laminar) or 25 s (turbulent).

As shown in Table 1, fraction samples containing as low as 10 cfu ml^{-1} *E. coli* can be distinguished from the blank. This lower detection limit is much lower than the other similar attempts and comparable to our previous study (Han et al., 2008). This sensitivity, however, is overestimated because dead cells and free antigens can also bind to anti-*E. coli* that cause agglutination and increase microfluidic signal (Nocker and Camper, 2006; Han et al., 2008). The dead cells and free antigen does not contribute to the number of colonies in cfu ml^{-1} unit obtained by conventional, cell culturing method. In this study, the ratio of dead and viable *E. coli* at peak point is approximately 4:1 in both laminar and turbulent flow (4.7×10^6 non-viable and 1.1×10^6 viable cells per ml in laminar flow; 60×10^6 non-viable and 13×10^6 viable cells per ml in turbulent flow). A considerable amount of dead cells and free antigens contributes to the microfluidic signals.

3.2. Axial dispersion of E. coli

Fig. 5 (a) and (b) presents the signals/data from microfluidic signals, viable *E. coli* counts, and electric conductivity meter (for salt concentration) against time for laminar and turbulent flows, respectively. All data are normalized, i.e. microfluidic signals and viable *E. coli* counts are divided by their maximum values, and the time is divided by the time when the signal reached its peak. The dimensionless times ($T = 4D \cdot t / d^2$; D = 2×10^{-9} m^2 s^{-1}, d = 1.6 cm and t = 300 s for laminar or 42 s for turbulent flow) are 9.4×10^{-3} for laminar and 1.3×10^{-3} for turbulent flow, which are mostly common in a pipe network ($T < 0.01$; Li et al., 2006). For laminar flow, microfluidic signals and salt concentrations showed asymmetric profiles (i.e. tailing from a symmetric, bell-shaped curve) against time, but viable *E. coli* counts show a symmetric profile trend tailing 20 minutes after

breakthrough. The asymmetric profile in laminar flow is caused by axial convection (i.e. transporting the solute toward downstream and spreading it as a result of the non-uniform velocity distribution), axial diffusion (molecules diffusing to the same direction with the main pipe flow), and radial diffusion (molecules diffusing perpendicular to the direction of main pipe flow) (Shanker and Lenhoff, 1989; Ekambara and Joshi, 2003, 2004). All three can be lumped together as axial dispersion. The microfluidic signals represent the total amount of *E. coli*, including viable cells and non-viable cell fragments/free antigens. The results for laminar flow clearly thus indicate that the axial dispersion is an issue of cell fragments and free antigens, but not viable cells, at least for *E. coli*.

For turbulent flow, all three curves show symmetric profiles while comparing with that of laminar flow, indicating there exist no axial dispersion phenomena for viable *E. coli* cells, cell fragments and free antigens from non-viable *E. coli*, and salt tracer, at least at Re = 6144.

3.3. CFD simulations

In section 3.2, microfluidic signals and salt tracer profiles show very similar trends in both laminar and turbulent flows. Based on this similarity, axial dispersion of *E. coli* is numerically simulated with CFD method, treating the *E. coli* solution (viable cells + cell fragments and free antigens) as a mixture of water (ρ = 998 kg m^{-3}, molecular weight = 18.01 g mol^{-1}) and salt (ρ = 2,170 kg m^{-3}, molecular weight = 58.48 g mol^{-1}). The density of salt in water is determined by the function of volume-weighted-mixing-law. Dynamic viscosity is set to that of water, 1 cP or 0.001 Pa s (Romero et al., 2008). A

Molecular diffusivity is set to that of salt, 1.5×10^{-9} m^2 s^{-1}. Salt concentration measured by conductometer at upstream end is used as initial inlet values for the simulation.

Fig. 5 (c) and (d) shows initial concentration profile at the inlet and final predicted results at the outlet by 2-D CFD models. Concentration values are normalized using maximum value at the inlet. In laminar flow (Re = 1,102), concentration profile at upstream end is symmetric (i.e. bell shape) and subsequently changes to asymmetric shape after certain time showing 89 % lower peak while compared to that at upstream end. In case of turbulent flow (Re = 6,144), however, symmetric profile does not significantly change between upstream and downstream end with 4.6 % difference between two peaks. Concentration profile estimated by EPANET shows however negligible differences compared to that at the inlet in laminar flow. EPANET shows its limitation for predicting axial dispersion of species in a pipe flow.

The predicted concentration profiles at the downstream end by 2-D CFD model are compared to results of section 3.2 for both laminar (Re = 1,102) and turbulent (Re = 6,144) flows, respectively as shown in fig 5 (a) and (b). All data are normalized with the same way presented in section 3.2. In laminar flow, predicted results show good agreement with microfluidic signals indicating 1-57% of error for the entire range of time. Much lower errors of 2-28% occur between the breakthrough to the peak point, 3-28%. In turbulent flow (Re = 6,144), predicted results show 10-37% of error for the entire range of time. The CFD model using property of salt as boundary condition suggests the possibility of numerical simulation for the behaviour of *E. coli* in a water distribution system.

4. Conclusion

The use of opto-microfluidic system is demonstrated for detecting *E. coli* in a pipe flow (laminar and turbulent). Latex immunoagglutination assays are performed and optically quantified in a microfluidic device (Fig. 2). Detection can be made in real time (<5 min per each assay) and at extremely low detection limit (10 cfu ml^{-1}), suggesting that the system is appropriate for monitoring waterborne pathogens in a water distribution system. Cell fragments and free antigens of *E. coli* behave similar to salt tracer (axial dispersion), while viable *E. coli* cells behave very differently (with no axial dispersion). Further, 2-D CFD model shows the possibility of modelling the behaviour of waterborne pathogens in a water distribution system.

Acknowledgments

The authors are grateful to Micro/Nanofabrication Center at the University of Arizona for the cleanroom facility and subsequent equipment assistance. This work was funded by the U.S. National Science Foundation (NSF) award no. EEC-0600855. We also thank all members in Water Distribution Network Laboratory at the University of Arizona for the experimental assistance in a pipe injection system and running CFD simulation.

Nomenclature

C	concentration of species	Sc_t	Schmidt number
$C_{1\varepsilon}$	turbulent model constant	t	Time
$C_{2\varepsilon}$	turbulent model constant	u^i	fluid velocity
$C_{3\varepsilon}$	turbulent model constant	x^i	Cartesian co-ordinate system
C_μ	turbulent model constant	μ	dynamic viscosity
G_k	generation of turbulence kinetic energy due to mean velocity gradient	μ_t	turbulent viscosity
J	diffusion flux of species	ρ	fluid density
k	turbulent kinetic energy	ε	turbulence dissipation rate
p	fluid pressure	σ_k	turbulent Prandtl number for k
R	mass rate of creation	σ_ε	turbulent Prandtl number for ε
Re	Reynolds number		

Table 1. Viable *E. coli* counts and microfluidic signals (mean ± standard deviation from three different measurements). * = significant difference from a blank signal ($p<0.05$) with *t*-tests; RSD = relative standard deviation.

Laminar			Turbulent		
Time (s)	*E. coli* cell count (cfu ml^{-1})	Microfluidic signal	Time (s)	*E. coli* cell count (cfu ml^{-1})	Microfluidic signal
Blank		1217±2	Blank		1253±8
65	10	1225±4*	17	0	1260±20
71	10	1232±4*	19	0	1271±5
77	30	1277±2*	21	4.84×10^{4}	1540±20*
83	1.20×10^{4}	1740±40*	23	9.87×10^{5}	1670±30*
89	2.60×10^{4}	2350±40*	25	1.26×10^{7}	1940±50*
95	1.97×10^{5}	3040±40*	27	9.98×10^{6}	2100±90*
101	2.00×10^{5}	3540±20*	29	3.12×10^{6}	1610±80*
107	2.31×10^{5}	3930±50*	31	2.25×10^{5}	1390±50*
113	2.31×10^{5}	3950±70*	33	5.82×10^{4}	1340±40*
119	6.49×10^{4}	3850±70*	36	8.51×10^{3}	1313±7*
140	1.07×10^{4}	3400±140*	42	985	1250±30*
160	1.02×10^{4}	3230±20*			
230	6.83×10^{3}	1910±20*			
300	2.99×10^{3}	1282±6*			
RSD (%)		0-4	RSD (%)		0-2

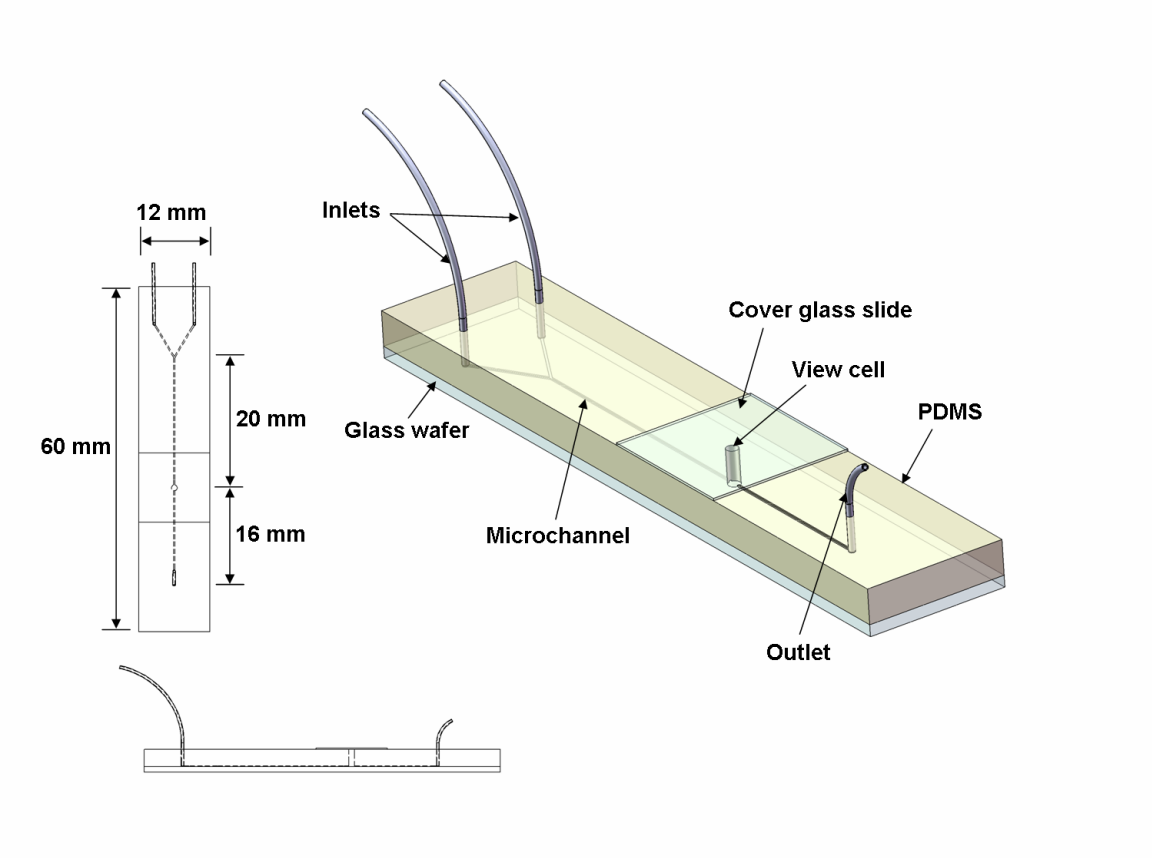

Fig 1. A schematic of Y-channel microfluidic device made out of polydimethylsiloxane (PDMS) molding technique

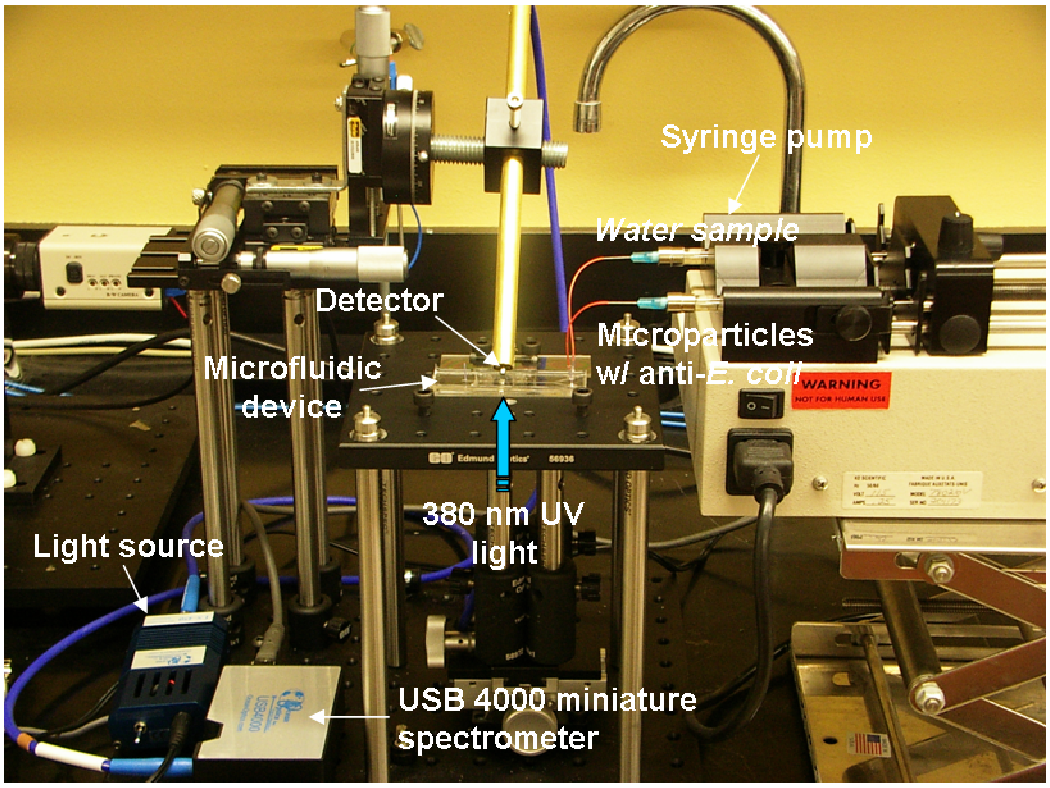

Fig. 2. A microfluidic device and proximity optical fibers on micro-positioning stages, with a portable spectrometer and UV (380 nm) light source.

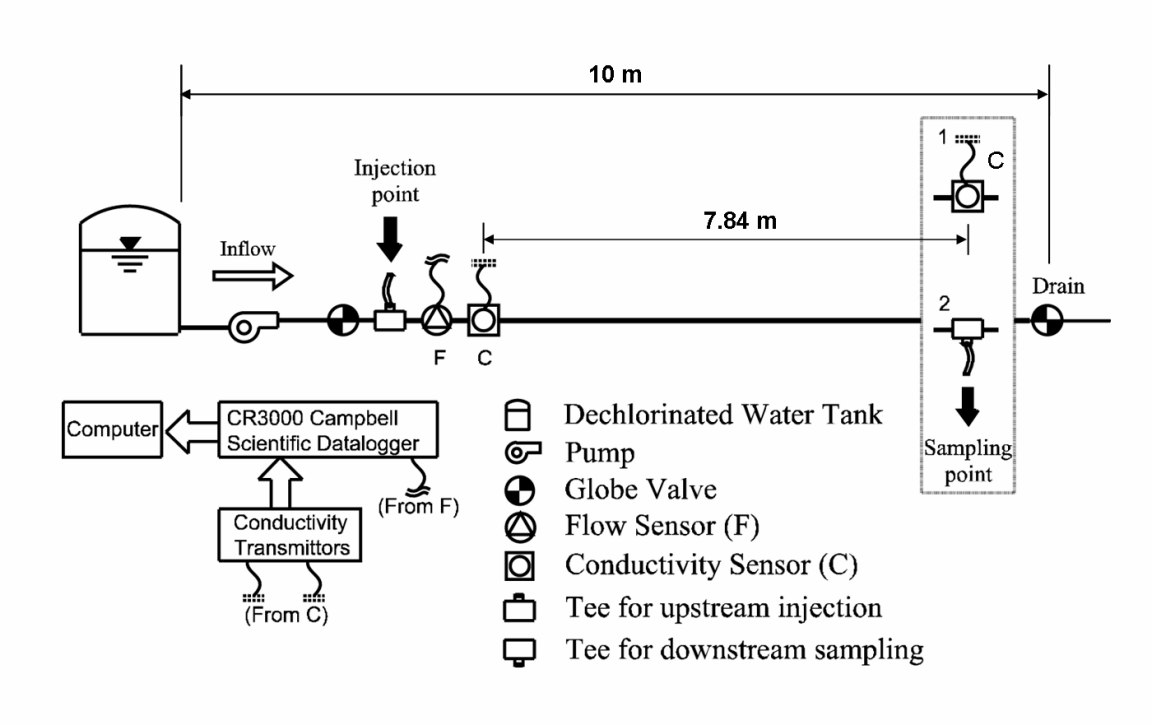

Fig. 3. Schematic of a straight pipe system.

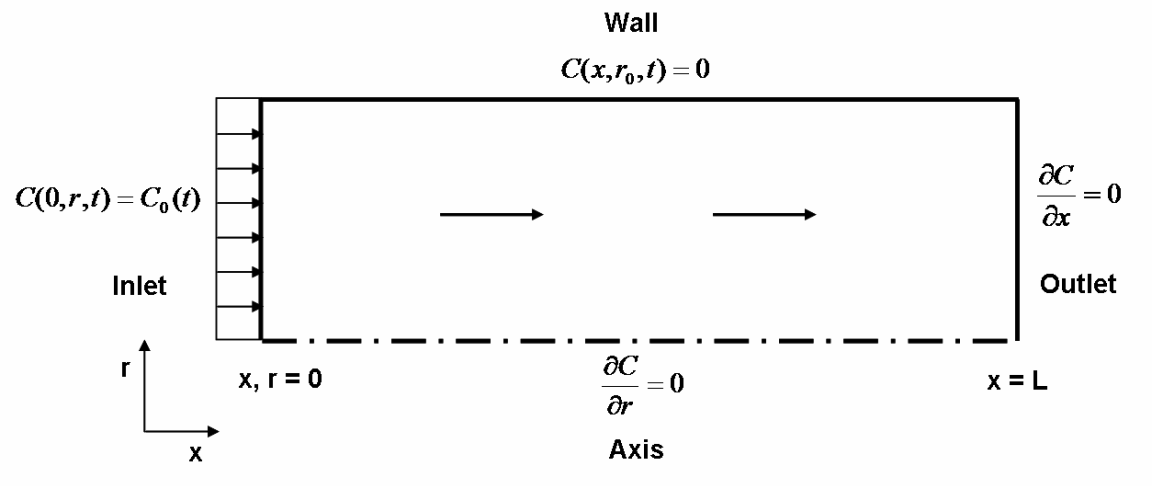

Fig. 4. Axi-symmetric geometry for 2-D CFD model; L = 7.48 m, D = 0.016 m, $0 \le x \le L$, $0 \le r \le \frac{D}{2}$.

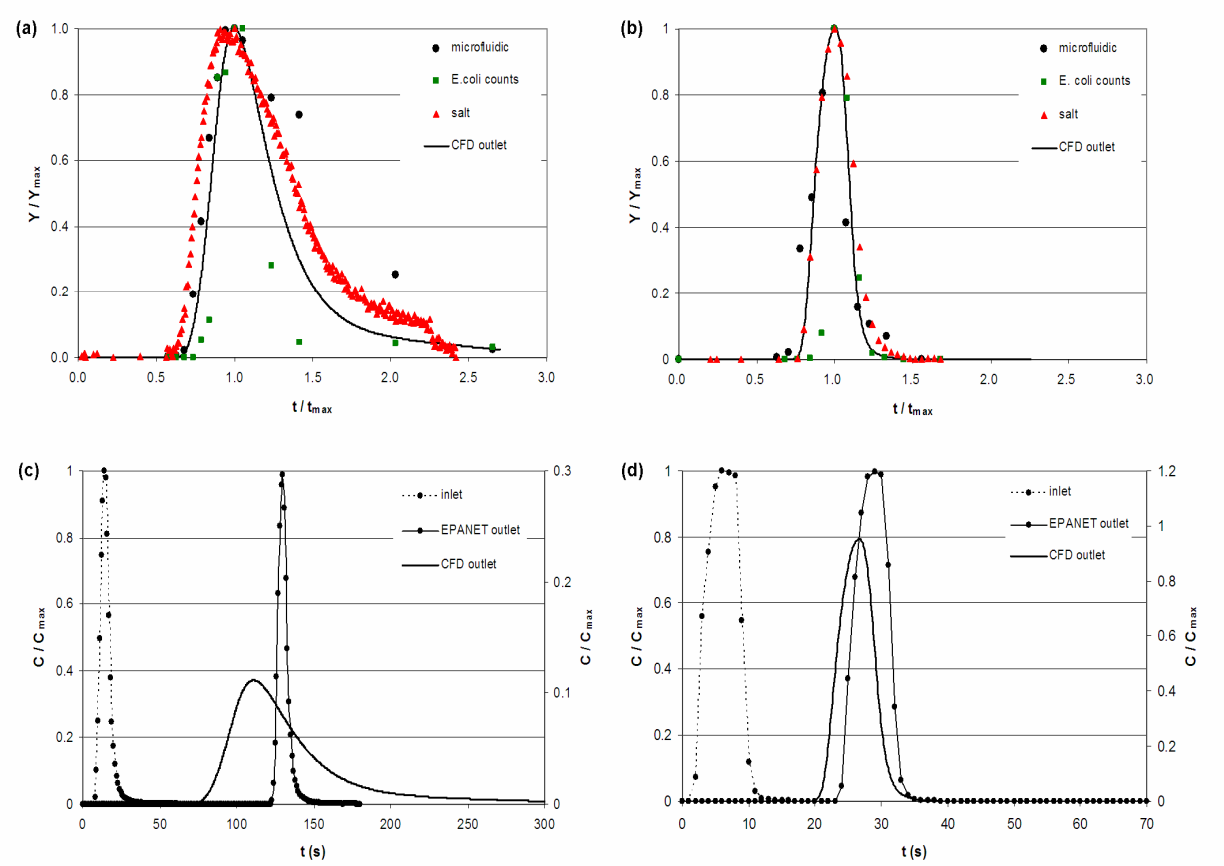

Fig. 5. Axial dispersion in laminar and turbulent flow; Comparison of dimensionless values of light scattering signals from a microfluidic device ("microfluidic"), viable cell counts of *E. coli* ("*E. coli* counts"), and the electrical conductivity representing the salt concentration ("salt"), as a function of dimensionless time at (a) Re = 1,102 and (b) Re = 6,144, (c) dimensionless concentration predicted by a 2-D CFD model and EPANET as a function of time at (c) Re = 1,102 and (d) Re = 6,144.

References

Ahmad A L; Lau K K (2007). Modeling, simulation, and experimental validation for aqueous solutions flowing in nanofiltration membrane channel. Industrial & Engineering Chemistry Research, 46(4), 1316-1325

Bangs L (1999). TechNote #204: Adsorption to Microspheres. Bangs Laboratories, Fishers, IN, USA

Berg H C (2004). *E. coli* in motion, In: Biological and Medical Physics, Biomedical Engineering, 56pp. Springer, New York, NY, USA

Cebeci T (2003). Turbulence models and their application, 5pp. Springer, New York, NY, USA

Ekambara K; Joshi J B (2003). Axial mixing in pipe flows: turbulent and transition regions. Chemical Engineering Science, 58(12), 2715-2724

Ekambara K; Joshi J B (2004). Axial mixing in laminar pipe flows. Chemical Engineering Science, 59(18), 3929-3944

Fluent Inc (2005). FLUENT 6.2 User's Guide. Fluent Inc., Lebanon, NH, USA

Han J H; Heinze B C; Yoon J Y (2008). Single cell level detection of *Escherichia coli* in a microfluidic device. Biosensors and Bioelectronics, 23(8), 1303-1306

Han J H; Kim K S; Yoon J Y (2007). The enhanced diffusional mixing for latex immunoagglutination assay in a microfluidic device. Analytica Chimica Acta, 584(2), 252-259

Hancu S; Ghinda T; Ma L; Lesnic D; Ingham D B (2002). Numerical modeling and experimental investigation of the fluid flow and contaminant dispersion in a channel.

International Journal of Heat and Mass Transfer, 45(13), 2707-2718

Khalizov A F; Earle M E; Johson W J W; Stubley G D; Sloan J J (2006). Modeling of flow dynamics in laminar aerosol flow tubes. Journal of Aerosol Science, 37(10), 1174-1187

Kieffer R; Charcosset C; Puel F; Magin D (2008). Numerical simulation of mass transfer in a liquid-liquid membrane contactor for laminar flow conditions. Computers and Chemical Engineering, 32, 1325-1333

Lin F Y H; Sherman P M; Li D (2004). Development of a novel hand-held immunoassay for the detection of enterohemorrhagic *Escherichia coli* O157:H7. Biomedical. Microdevices, 6(2), 125-130

Li Y; Su X L (2006). Simultaneous detection of *Eshcerichia coli* O157:H7 and *Salmonella typhimurium* using quantum dots as fluorescence labels. Journal of Rapid Methods and Automation in Microbiology, 14(1), 96-109

Lomax H; Pulliam T H; Zingg D W (2003). Fundamentals of computational fluid dynamics, 7pp. Springer, New York, NY, USA

Nallasamy M (1987). Turbulence models and their applications to the prediction of internal flows – review. Computers and Fluids, 15(2), 151-194

Nocker A; Camper A H (2006). Selective removal of DNA form dead cells of mixed bacterial communitites by use of ethidium monoazide. Applied and Environmental Microbiology, 72(3), 1997-2004

Romero-Gomez P; Ho C K; Choi C Y (2008). Mixing at Cross Junctions in Water Distribution Systems - Part I. A numerical study. ASCE Journal of Water Resources Planning and Management, 134(3), 284-294

Shankar A; Lenhoff A M (1989). Dispersion in laminar flow in short tubes. AIChE Journal, 35, 2048-2052

Stovin V R; Saul A J (1998). A computational fluid dynamics (CFD) particle tracking approach to efficiency prediction. Water Science and Technology, 37(1), 285-293

Taylor G I (1953). Dispersion of soluble matter in solvent flowing slowly through a tube. Proceedings Royal Society of London, Series A, 219(1137), 186-203

Taylor G I (1954). The dispersion of matter in turbulent flow through a pipe, Proceedings Royal Society of London, Series A, 223(1155), 446-468

Wilkening H; Baraldi D (2007). CFD modeling of accidental hydrogen release from pipelines. International Journal of Hydrogen Energy, 32(13), 2206-2215

Xia Y; Whitesides G M (1998). Soft lithography. Annual Review of Materials Science, 28(1), 153–184